

# **Fabrication of lithium silicates from SBA-15 with superior CO<sub>2</sub> capture performance**

Yirong Pan<sup>1</sup>, Qianwen Zheng<sup>1</sup>, Qingqing Qin<sup>1</sup>, Yu Zhang<sup>1</sup>, Wanlin Gao<sup>1</sup>, Liang Huang<sup>1</sup>, Tuantuan Zhou<sup>1</sup>, Benoît Louis<sup>2</sup>, Dermot O'Hare<sup>3</sup>, Qiang Wang<sup>1,\*</sup>

<sup>1</sup>College of Environmental Science and Engineering, Beijing Forestry University, 35 Qinghua East Road, Haidian District, Beijing 100083, P. R. China.

<sup>2</sup>Laboratoire de Synthèse, Réactivité Organiques et Catalyse, Institut de Chimie, UMR 7177, Université de Strasbourg, 1 rue Blaise Pascal, 67000 Strasbourg, France

<sup>3</sup>Chemistry Research Laboratory, Department of Chemistry, University of Oxford, Mansfield Road, Oxford OX1 3TA, United Kingdom

## **Corresponding author:**

College of Environmental Science and Engineering, Beijing Forestry University, 35 Qinghua East Road, Haidian District, Beijing 100083, China

E-mail: [qiang.wang.ox@gmail.com](mailto:qiang.wang.ox@gmail.com); [qiangwang@bjfu.edu.cn](mailto:qiangwang@bjfu.edu.cn)

Tel: +86-13699130626

## Abstract

A series of lithium silicates with improved CO<sub>2</sub> sorption capacity were successfully synthesized using SBA-15 as the silicon precursor. The influence of Li/Si ratio, calcination temperature, and calcination duration on the chemical composition and the CO<sub>2</sub> capture capacity of obtained lithium silicates were systematically investigated. The correlation between the CO<sub>2</sub> sorption performance and the crystalline phase abundance was determined using X-ray diffraction and a normalized reference intensity ratio method. Under the optimized conditions, the Li-SBA15-4 sample that mainly contains Li<sub>4</sub>SiO<sub>4</sub> achieved an extremely high CO<sub>2</sub> capture capacity of 36.3 wt% (corresponding to 99% of the theoretical value of 36.7 wt% for Li<sub>4</sub>SiO<sub>4</sub>), which is much higher than the Li<sub>4</sub>SiO<sub>4</sub> synthesized from conventional SiO<sub>2</sub>. It also showed very high cycling stability with only 1.0 wt% capacity loss after 15 cycles. The Li-SBA15-10 sample that mainly contains Li<sub>8</sub>SiO<sub>6</sub> displayed an amazingly high CO<sub>2</sub> uptake of 62.0 wt%, but its regeneration capacity was poor, with only 10.5 wt% of reversible CO<sub>2</sub> capture capacity. The influence of CO<sub>2</sub> concentration on the CO<sub>2</sub> capture performance of Li-SBA15-4 and Li-SBA15-10 samples was also studied. With the decrease in CO<sub>2</sub> concentration, relatively lower temperatures are needed for its maximum CO<sub>2</sub> capture capacity. The CO<sub>2</sub> sorption kinetics and mechanism for Li-SBA15-4 and Li-SBA15-10 samples were explored. In all, we have demonstrated that the lithium silicates synthesized from SBA-15 could result in much improved CO<sub>2</sub> sorption performance than those from conventional SiO<sub>2</sub>.

**Keywords:** Li<sub>4</sub>SiO<sub>4</sub>; Li<sub>8</sub>SiO<sub>6</sub>; SBA-15; alkali silicate-based sorbents; sorption enhanced hydrogen production; global warming

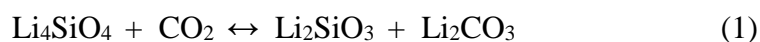
## 1. Introduction

CO<sub>2</sub> is one of the major greenhouse gases that contribute significantly to global warming and its capture is an important pre-requisite step for the following CO<sub>2</sub> storage or utilizations. Using solid adsorbents/sorbents to capture CO<sub>2</sub> is promising and the solid adsorbents/sorbents can be classified as low-temperature (<200 °C), intermediate-temperature (200–400 °C), and high-temperature (>400 °C) adsorbents/sorbents according to their working temperature ranges.<sup>1, 2</sup>

High-temperature CO<sub>2</sub> sorbents are mainly used in the sorption enhanced steam methane reforming process which operates at between 500 and 800 °C. With these sorbents, the conversion of methane to H<sub>2</sub> can be improved, and in the meantime, pure CO<sub>2</sub> can be captured.<sup>3</sup> Up to date, several types of high-temperature CO<sub>2</sub> sorbents have been developed such as CaO-based, alkali dititanates, alkali zirconates, and alkali silicates, *etc.*<sup>4-7</sup> Alkali silicate-based sorbents have attracted tremendous attention owing to their high CO<sub>2</sub> capture capacity and lower regeneration temperature. A series of alkali silicate-based sorbents including Li<sub>4</sub>SiO<sub>4</sub>, Li<sub>4-x</sub>Na<sub>x</sub>SiO<sub>4</sub>, Li<sub>4+x</sub>(Si<sub>1-x</sub>Al<sub>x</sub>)O<sub>4</sub>, Li<sub>8</sub>SiO<sub>6</sub>, Li<sub>6</sub>Si<sub>2</sub>O<sub>7</sub>, Li<sub>2</sub>Si<sub>2</sub>O<sub>5</sub>, Li<sub>2</sub>Si<sub>3</sub>O<sub>7</sub>, CaSiO<sub>3</sub>, and (OH)<sub>3</sub>Al<sub>2</sub>O<sub>3</sub>SiOH have been studied for CO<sub>2</sub> sorption.<sup>8</sup> Among various alkali silicate-based sorbents, Li<sub>4</sub>SiO<sub>4</sub> and Li<sub>8</sub>SiO<sub>6</sub> are the topic of significance owing to their elevated CO<sub>2</sub> sorption capacity and kinetics.

Li<sub>4</sub>SiO<sub>4</sub> was found to possess outstanding CO<sub>2</sub> sorption property about 15 years ago.<sup>9</sup> During CO<sub>2</sub> sorption process, a reversible reaction can readily occur as shown in equation (1). The theoretical CO<sub>2</sub> capture capacity of Li<sub>4</sub>SiO<sub>4</sub> can be calculated straightforwardly as 36.7 wt%. During the past few years, great effort has been devoted

to the improvement of CO<sub>2</sub> uptake and cycling stability of Li<sub>4</sub>SiO<sub>4</sub>. For this sake, several attempts have been carried out such as searching for suitable silicon sources, loading with alkali metals, designing unique morphology, *etc.* Some alkali silicate-based sorption materials and their CO<sub>2</sub> capture performance are summarized at Table 1.



Olivares-Marín *et al.*<sup>10</sup> developed Li<sub>4</sub>SiO<sub>4</sub> from fly ash by a solid-state reaction and doped with K<sub>2</sub>CO<sub>3</sub>, and this novel sorbent resulted in a CO<sub>2</sub> uptake of 10.7 wt%. Ortiz-Landeros *et al.*<sup>11</sup> doped Li<sub>4</sub>SiO<sub>4</sub> with transition metals, aluminum and vanadium ions, and obtained a CO<sub>2</sub> uptake of 17.1 wt%. Shan *et al.*<sup>12</sup> prepared Li<sub>4</sub>SiO<sub>4</sub> from diatomite by a solid-state method, and the maximum CO<sub>2</sub> uptake of the sample increased to 28.6 wt% (78% of theoretical sorption capacity). Xiang *et al.*<sup>13</sup> used a sol-gel process to synthesis Li<sub>3.9</sub>Na<sub>0.1</sub>Si<sub>0.96</sub>Ti<sub>0.04</sub>O<sub>4</sub> porous sorbent and studied the relationship between Ti-doping and volume expansion for the first time, and the CO<sub>2</sub> uptake was increased to 31.6 wt% (86% of theoretical sorption value). Lee *et al.*<sup>14</sup> fabricated the coral-like Li<sub>4</sub>SiO<sub>4</sub> by thermal conversion of a Li- and Si- containing metal-organic framework, and the maximum CO<sub>2</sub> uptake reached 32.4 wt% at 550 °C. Wang *et al.*<sup>15</sup> used a sol-gel process to synthesize Li<sub>4</sub>SiO<sub>4</sub> coupled with carbon coating, and the sample possessed a high CO<sub>2</sub> capture capacity of 34.2 wt% (93% of theoretical sorption value). Subha *et al.*<sup>16</sup> used colloidal silica as the silicon source to prepare Li<sub>4</sub>SiO<sub>4</sub> by a sol-gel process, through which the CO<sub>2</sub> uptake of Li<sub>4</sub>SiO<sub>4</sub> was increased once again to 35.0 wt% (97% of theoretical sorption capacity). It was noteworthy that Durán-Muñoz *et al.*<sup>17</sup> successfully synthesized Li<sub>8</sub>SiO<sub>6</sub> with much higher CO<sub>2</sub> uptake

of 52.1 wt%.

SBA-15 is a typical type of molecular sieve with a chemical composition of silica. Owing to its mesopores ranging from 5 to 30 nm, uniform ordered mesoporous channels, and high specific surface area, SBA-15 has a vast application area and can be widely used as catalysts, catalyst supports, and adsorbents, *etc.*<sup>18</sup> It is not complex to obtain SBA-15 with different morphology and structure by changing synthesis parameters such as hydrothermal reaction duration, temperature and hydrochloric acid concentration, *etc.*<sup>19</sup> Thanks for its ordered pore channels, high specific surface area and thin wall thickness, we speculated that SBA-15 can lead to a much better contact with lithium precursors than commercial SiO<sub>2</sub> so that highly pure lithium silicates can be obtained after shorter calcination duration and lower calcination temperatures. However, to date, there is no report has used SBA-15 as silica precursor for the fabrication of lithium silicates-based CO<sub>2</sub> sorbents. In this contribution, we aim to develop a series of lithium silicates from SBA-15 precursor and comprehensively investigate their CO<sub>2</sub> capture performance at high-temperatures.

## **2. Experimental**

### **2.1 Preparation of samples**

#### **2.1.1 Preparation of SBA-15**

SBA-15 was synthesized using a modified classical method.<sup>35</sup> First, 360 g deionized water was mixed with 43 g hydrochloric acid (36–38%, Beijing Chemical Works), followed by adding 12 g P-123 block copolymer (Sigma-Aldrich Life Science & Technology Co., Ltd.) into the solution. The mixed solution was stirred vigorously at

35 °C until P-123 dissolved completely, after which 24 g tetraethyl orthosilicate (Sinopharm Chemical Reagent Co., Ltd.) was added dropwise and kept stirring at 35 °C for 24 h. Second, the resulting gel was transferred into a Teflon-lined autoclave and kept at 100 °C for 24 h. Third, the product was filtered off and washed with deionized water until the filter liquor was neutral, and calcined at 550 °C for 6 h. After grinding, white powder of SBA-15 was obtained.

### **2.1.2 Preparation of lithium silicates**

For the synthesis of lithium silicates-based CO<sub>2</sub> sorbents, a solid-state reaction was implemented to load SBA-15 with lithium nitrate. 0.3 g synthesized SBA-15 powders and corresponding lithium nitrate (SHFS Co.) were mixed mechanically at a certain ratio in an agate mortar, and moderate absolute ethanol (99.8%, Beijing Chemical Works) was added in order to mix homogeneously during grinding process. After drying in the oven at 60 °C for several minutes, the mixed powders were calcined at 750 °C for 6 h. In this contribution, other calcination temperature and duration were also used for the optimization purpose. The molar ratio of Li/Si was controlled in a wide range of 3–11, and the correspondingly synthesized samples were noted as Li-SBA15-*x*, in which *x* represents the Li/Si ratios.

### **2.2 Characterizations of samples**

Powder X-ray diffraction (XRD) analysis was performed in a Shimadzu XRD-7000 instrument in reflection mode with Cu K $\alpha$  radiation and a power of 40 kV  $\times$  40 mA. Within a wide-angle range of  $2\theta = 5\text{--}80^\circ$ , XRD patterns were recorded with a scanning speed of 5° per minute and a step size of 0.02°. Within a low-angle range of  $2\theta = 0.5\text{--}$

5°, XRD patterns were recorded with a scanning speed of 1° per minute and a step size of 0.02°. To evaluate the pore size distribution and specific surface areas of samples, N<sub>2</sub> adsorption/desorption test was conducted in a BET instrument (SSA-7000). The morphology and structure characterizations of samples were examined using scanning electronic microscopy (SEM, Hitachi S-3400N II) and transmission electronic microscopy (TEM, JEM-1010) analyses.

### **2.3 Evaluation of CO<sub>2</sub> sorption performance**

CO<sub>2</sub> sorption capacity and cycling stability were both evaluated using a TGA apparatus (Q50 TA Instrument). Approximately 20 mg of the sample was loaded into a platinum tray and heated from room temperature to the sorption temperature at a ramping rate of 5 °C/min under pure N<sub>2</sub> atmosphere. After keeping at sorption temperature for 30 min, N<sub>2</sub> was shifted to CO<sub>2</sub> with different concentrations and the sample was left to sorb CO<sub>2</sub> for 180 min continuously. Cycling stability measurements were conducted with the similar conditions. CO<sub>2</sub> sorption was performed at 650 °C for 60 min and the desorption was performed at the same temperature for 30 min. During all evaluation processes, the flow rate of N<sub>2</sub> and CO<sub>2</sub> was kept at 40 and 20 mL/min, respectively.

## **3. Results and discussion**

### **3.1 Characterization of synthesized SBA-15**

The synthesized SBA-15 was thoroughly characterized using XRD, N<sub>2</sub> adsorption/desorption, SEM, and TEM analyses. Fig. 1(a) shows the XRD patterns of synthesis SBA-15 in both low-angle and wide-angle modes. In the low-angle pattern,

three peaks corresponding to the reflections of (100), (110), (200) planes were observed, which can be attributed to the hexagonal arrangement of the pores in SBA-15 and was consistent with literature reports.<sup>35,36</sup> The wide-angle XRD pattern of synthesized SBA-15 can be seen at the inset, and the broaden peak appeared at approximately 22° indicated that SBA-15 was a kind of amorphous silica. Fig. 1(b) shows the N<sub>2</sub> adsorption/desorption isotherm of synthesized SBA-15. The curves of adsorption and desorption were parallel and showed a H1-type hysteresis loop, which is the characteristic of a type IV isotherm, indicating that SBA-15 possessed regular and homogeneous mesopores.<sup>37</sup> Its specific surface area and pore size calculated by BET method was 907.0 m<sup>2</sup>/g and 5.6 nm, respectively.

The morphology and the mesoporous structure were then examined using SEM and TEM analyses. Fig. 1(c) shows the SEM image of synthesized SBA-15, which indicates a fiber rod-like morphology. The TEM image in Fig. 1(d) shows that the sample exhibits highly-ordered pore channels. In agreement with the XRD and BET analyses, it can be concluded that SBA-15 was successfully synthesized.

### **3.2 Optimization of the synthesis of lithium silicates**

A comprehensive investigation on the synthesis of a series of lithium silicates were conducted by changing the Li/Si ratio, calcination temperature, and calcination duration, etc. The influence of synthesis condition on the CO<sub>2</sub> sorption capacity of obtained samples was also studied. In order to correlate the CO<sub>2</sub> sorption capacity with their structure and the chemical composition, all samples were characterized using XRD and analyzed using a normalized reference intensity ratio (RIR) method. Thus, the



optimization of the synthesis of lithium silicates was based on both the CO<sub>2</sub> sorption capacity and the XRD and RIR analyses.

In order to determine the appropriate sorption temperature, the effect of sorption temperature on the CO<sub>2</sub> capture capacity of Li-SBA15-4 sample synthesized by calcining at 750 °C for 6 h was first investigated, as shown in Fig. 2(a). With the increase in sorption temperature from 550 to 700 °C, the CO<sub>2</sub> sorption capacity first increased from 550 to 650 °C and then started to decrease from 650 to 700 °C. It is obvious that the best CO<sub>2</sub> sorption temperature was 650 °C. Indeed, when the sorption temperature is low, it is not good for producing an eutectic mixture that can promote reactants diffusion.<sup>27</sup> However, too high sorption temperature will lead to sintering and possibly devitalizes the activation of reactants. Therefore, it is reasonable to select 650 °C as an optimal sorption temperature for further experiments to investigate the CO<sub>2</sub> capture performance of other samples.

### **3.2.1 The influence of Li/Si molar ratio**

The influence of Li/Si molar ratio on the formation of lithium silicates and their CO<sub>2</sub> sorption capacity was also explored, as shown in Fig. 2(b) and (c). In this section, all Li-SBA15-*x* (*x* = 3, 4, 5, 6, 7, 8, 9, 10, 11.) samples were synthesized at 750 °C for 6 h and were tested at 650 °C. For Li-SBA15-3 sample, the CO<sub>2</sub> sorption curve sharply increased to a plateau within 10 min. As the Li/Si molar ratio was increased to 4, the CO<sub>2</sub> sorption capacity of the sample was increased to 35.6 wt%, which corresponds to 97.1% of the theoretical value. With a further increase of Li/Si molar ratio from 5 to 7, the CO<sub>2</sub> sorption capacity of samples continuously increased but it took a longer

duration to reach a plateau in comparison with Li-SBA15-3 and Li-SBA15-4. A similar variation tendency was also clearly observed as the Li/Si molar ratio increased from 8 to 10, and the CO<sub>2</sub> uptake of Li-SBA15-10 sample tremendously increased up to 59.8 wt%. However, for Li-SBA15-11 sample, almost no change was observed in CO<sub>2</sub> sorption capacity comparing to that of Li-SBA15-10.

In order to correlate the CO<sub>2</sub> sorption capacity with the composition of sorbents, the chemical composition of samples with different Li/Si molar ratios were then determined using XRD and RIR analyses, as shown in Fig. 3 and Table 2. For Li-SBA15-3 and Li-SBA15-4 samples, Li<sub>4</sub>SiO<sub>4</sub> was the main phase and a certain amount of Li<sub>2</sub>SiO<sub>3</sub> can be detected definitely at 18.84° and 26.92°. However, as the ratio was increased to 5, only the main characteristic peak of Li<sub>4</sub>SiO<sub>4</sub> was observed at 22.14°, which indicated that pure Li<sub>4</sub>SiO<sub>4</sub> phase was obtained. Comparing to Li-SBA15-4, its CO<sub>2</sub> sorption capacity was slightly lower (Fig. 2(c)). This might be due to Li<sub>2</sub>SiO<sub>3</sub> impurity in Li-SBA15-4 which can act as a well lithium ion conductor, promoting the bulk diffusion.<sup>38</sup> With the increase in Li/Si molar ratio, the Li<sub>4</sub>SiO<sub>4</sub> phase was always detected, and in the meantime, Li<sub>8</sub>SiO<sub>6</sub> phase (25.24°) started to appear in Li-SBA15-6 sample. Furthermore, the LiOH phase was also observed at around 32.50° in Li-SBA15-9 and SBA15-10 samples. Owing to the existence of Li<sub>8</sub>SiO<sub>6</sub> and LiOH, the CO<sub>2</sub> sorption capacity of these samples was significantly increased. Nevertheless, with the ratio was increased to 11, the characteristic reflection of LiOH was replaced by that of Li<sub>2</sub>O at 33.44°, which was in agreement with the CO<sub>2</sub> uptake variation that the CO<sub>2</sub> uptake of Li-SBA15-11 sample was slightly higher than that of Li-SBA15-10 sample.

Because  $\text{Li}_2\text{O}$  possesses a higher theoretical capacity than  $\text{LiOH}$ .

By far, it is still a mystery why some samples have the same chemical composition but different sorption capacities. So we further analyzed the XRD patterns of all samples using a normalized RIR method, as given by equation (2).<sup>39, 40</sup> This is aimed to achieve a deeper understanding of the intrinsic reason that how the Li/Si molar ratio influences the  $\text{CO}_2$  sorption performance, with regard on crystalline phase abundance. In equation (2),  $x$  means one phase in the all definite crystalline phases of the analyzed sample and  $W_x$  represents the phase abundance of  $x$  phase.  $A$  is representative for the phase selected to work as an internal standard, and  $I_x$  denotes the intensity of a specific pattern of  $x$  phase which can be obtained from the peak reported in Jade analysis software. Finally,  $K_A^x$  can be calculated from equation (3). In this equation,  $K_x$  is equal to the RIR value of  $x$  phase, which can be referred as the relevant PDF card. All calculated results were summarized in Table 2 in a percentage form.

$$W_x = \left( \frac{K_A^x}{I_x} \sum_{i=A}^n \frac{I_i}{K_A^i} \right)^{-1} \quad (2)$$

$$K_A^x = \frac{K_x}{K_A} \quad (3)$$

Table 2 shows that the  $\text{CO}_2$  sorption capacity of Li-SBA15-3 and Li-SBA15-4 samples increased with the growth of  $\text{Li}_4\text{SiO}_4$  phase abundance. It was noteworthy that the  $\text{Li}_4\text{SiO}_4$  phase abundance amazingly attained 98 wt% in the ratio 4. For comparison purpose, the sample with the same Li/Si ratio of 4 was also synthesized using  $\text{SiO}_2$  powder rather than SBA-15 as the silicon precursor. The  $\text{Li}_4\text{SiO}_4$  phase abundance was only around 80 wt% in this control sample. In the conventional synthesis process,<sup>3, 20, 22, 23, 29, 31</sup> it is common to add excess lithium for preventing the sublimation. In the same

synthesis method, SBA-15 as a silicon source produced a much pure  $\text{Li}_4\text{SiO}_4$  phase, which may be attributed to its ordered mesoporous structure that promoted lithium dispersion and complete reaction. For Li-SBA15-5 sample, only  $\text{Li}_4\text{SiO}_4$  phase can be detected and its abundance was calculated as 100 wt%. With increase in Li/Si molar ratio,  $\text{Li}_8\text{SiO}_6$ ,  $\text{LiOH}$ , and  $\text{Li}_2\text{O}$  phases with higher theoretical sorption values appeared in sequence. The  $\text{CO}_2$  uptake of Li-SBA15-6 and Li-SBA15-7 samples increased with the increase in the  $\text{Li}_8\text{SiO}_6$  phase abundance. However, the  $\text{Li}_8\text{SiO}_6$  phase abundance confusingly decreased in Li-SBA15-8 sample so that its  $\text{CO}_2$  uptake also reduced. For Li-SBA15-9 and Li-SBA15-10 samples, their  $\text{CO}_2$  uptake also increased owing to the increase in both  $\text{Li}_8\text{SiO}_6$  and  $\text{LiOH}$  phase abundances. As the Li/Si molar ratio was increased to 11, the  $\text{Li}_8\text{SiO}_6$  phase abundance further increased and a small amount of  $\text{Li}_2\text{O}$  phase was observed, by which the  $\text{CO}_2$  sorption capacity slightly increased. According to the chemical composition and  $\text{CO}_2$  sorption capacity, Li-SBA15-4 sample mainly containing  $\text{Li}_4\text{SiO}_4$  and Li-SBA15-10 sample mainly containing  $\text{Li}_8\text{SiO}_6$  were selected as exceptional sorbents for further studies.

### **3.2.2. The influence of calcination duration**

The influence of calcination duration of Li-SBA15-4 and Li-SBA15-10 samples was further optimized by fixing at the calcination temperature of 750 °C. Fig. 4(a) shows that the  $\text{CO}_2$  sorption capacity of Li-SBA15-4 samples first increased and then decreased with the increase of calcination duration from 0.5 to 6 h. The highest  $\text{CO}_2$  sorption capacity of 36.3 wt%, corresponding to 99% of its theoretical value, was obtained with the sample calcined for 2 h. It was noteworthy that material fabricated

from SBA-15 still exhibited a high CO<sub>2</sub> uptake even the calcination duration was as short as 0.5 h. In Fig. 4(a), the dash line stands for the CO<sub>2</sub> sorption curve of the sample synthesized from SiO<sub>2</sub> at 750 °C for 2 h. Apparently the CO<sub>2</sub> uptake (only 23.5 wt%) of the sample synthesized from SiO<sub>2</sub> was much less than that from SBA-15.

According to Fig. 4(b), the CO<sub>2</sub> sorption capacity of Li-SBA15-10 samples displayed the similar variation trend than Li-SBA15-4 samples. What's more, the weight dramatically increased in a very short time within 2 min and the highest capacity of 62.0 wt% belonged to the sample calcined for 4 h. For comparison, a control sample from SiO<sub>2</sub> was synthesized under the same conditions (750 °C for 4 h) of the Li-SBA15-10 sample with the highest CO<sub>2</sub> uptake. It is clear that its CO<sub>2</sub> sorption capacity is much less than that of the sample prepared from SBA-15 under the same synthesis condition, which is only 50.5 wt%.

Fig. 4(c) and (d) show the XRD pattern of Li-SBA15-4 and Li-SBA15-10 samples with different calcination durations, respectively. For Li-SBA15-4 pristine samples, all calcinations led to mainly Li<sub>4</sub>SiO<sub>4</sub> phase and tiny Li<sub>2</sub>SiO<sub>3</sub> phase, whose Li<sub>4</sub>SiO<sub>4</sub> phase abundance first decreased and then increased as calcination duration decreased from 6 to 0.5 h and the lowest value was obtained for sample calcined for 2 h (Table 2). As a well lithium ions conductor, Li<sub>2</sub>SiO<sub>3</sub> can improve the CO<sub>2</sub> sorption property of the samples. Hence, moderate phase abundance of Li<sub>4</sub>SiO<sub>4</sub> and Li<sub>2</sub>SiO<sub>3</sub> phase may be the reason why the sample calcined for 2 h possesses the highest CO<sub>2</sub> sorption capacity. Compared with the above-mentioned samples, the sample synthesized from SiO<sub>2</sub> by calcining for 2 h contained much less Li<sub>4</sub>SiO<sub>4</sub> and relatively a big amount of SiO<sub>2</sub> still

existed in the sample. This indicates that the reaction between silicon source and lithium nitrate was incomplete, which resulted in a relatively low CO<sub>2</sub> sorption capacity. For Li-SBA15-10 samples, all samples contained Li<sub>8</sub>SiO<sub>6</sub>, Li<sub>4</sub>SiO<sub>4</sub> and LiOH phase, but the abundance of each phase was different. As the calcination duration decreased from 6 to 0.5 h, Li<sub>8</sub>SiO<sub>6</sub> first increased and then sharply decreased. The sample calcined for 4 h possessed the maximum Li<sub>8</sub>SiO<sub>6</sub> phase abundance and the highest CO<sub>2</sub> sorption capacity.

### **3.2.3. The influence of calcination temperature**

The calcination temperature for the synthesis of lithium silicates was further optimized based on the selected Li/Si molar ratio and calcination duration. At different calcination temperatures, the Li-SBA15-4 and Li-SBA15-10 samples were calcined for 2 and 4 h, respectively. Fig. 5(a) and (b) show the CO<sub>2</sub> sorption isotherms of Li-SBA15-4 and Li-SBA15-10 samples obtained at different calcination temperatures. The results indicate that 750 °C is the optimal calcination temperature for both samples, which resulted in the highest CO<sub>2</sub> sorption capacity.

The XRD patterns and phase abundances of these samples are shown in Fig. 5(c) and (d) and Table 2. For Li-SBA15-4 samples, all the samples calcined at different temperatures consisted of Li<sub>4</sub>SiO<sub>4</sub> and Li<sub>2</sub>SiO<sub>3</sub> phases. The sample calcined at 750 °C contained slightly more Li<sub>2</sub>SiO<sub>3</sub>, which might be the reason for its better CO<sub>2</sub> capture performance. For Li-SBA15-10 samples, in addition to Li<sub>8</sub>SiO<sub>6</sub> and Li<sub>4</sub>SiO<sub>4</sub>, LiOH and Li<sub>2</sub>O formed in sequence as the calcination temperature raised from 650 to 850 °C. In addition, the sample containing high Li<sub>8</sub>SiO<sub>6</sub> phase abundance showed the highest CO<sub>2</sub>

sorption capacity (Fig. 5(b) and Table 2).

Fig. 6 shows the comparison of the CO<sub>2</sub> capture capacity of our synthesized Li<sub>4</sub>SiO<sub>4</sub> (noted as Li-SBA15-4) with some recent literature reports. It can be seen that with the great effort performed by various researchers, the CO<sub>2</sub> capture capacity of Li<sub>4</sub>SiO<sub>4</sub> was increased step by step from 28.6 wt% to 35 wt%, corresponding to 78% to 95% of the theoretical uptake of Li<sub>4</sub>SiO<sub>4</sub> (36.67 wt%). To the best of our knowledge, prior to our present work, the highest CO<sub>2</sub> uptake for Li<sub>4</sub>SiO<sub>4</sub> was 35 wt%.<sup>12-16</sup> However, in this contribution, the CO<sub>2</sub> uptake of Li<sub>4</sub>SiO<sub>4</sub> (Li-SBA15-4) that we synthesized from SBA-15 precursor was further increased to 36.3 wt%, corresponding to 99% of its theoretical CO<sub>2</sub> uptake. In addition, the Li<sub>8</sub>SiO<sub>6</sub> (Li-SBA15-10) that we synthesized similarly from SBA-15 precursor also resulted in a higher CO<sub>2</sub> uptake (62.0 wt%) comparing to previous literature reports.<sup>17, 34</sup> Therefore, these two superior sorbents Li-SBA15-4 and Li-SBA15-10 were further investigated comprehensively in the following sections.

### **3.3 Characterization of optimized lithium silicates sorbents**

The microstructural information of two optimized samples of the Li-SBA15-4 sample synthesized at 750 °C for 2 h and the Li-SBA15-10 sample synthesized at 750 °C for 4 h were carefully characterized by N<sub>2</sub> adsorption/desorption isotherms and SEM analysis. As shown in Fig. 7(a) and (b), according to the IUPAC, both samples presented a type III isotherm with the narrow H3 hysteresis loops in a wide relative pressure range, corresponding to a non-porous or macroporous material. The BET specific surface areas of both samples were quite low, being 1.0 and 1.5 m<sup>2</sup>·g<sup>-1</sup> for Li-SBA15-4 and Li-

SBA15-10, respectively. This data indicated that the ordered mesoporous structure of SBA-15 disappeared, which can be explained by the high temperature sintering during solid-state reactions.<sup>15, 23</sup> To elucidate this hypothesis, the optimized Li-SBA15-4 and Li-SBA15-10 samples were characterized using SEM analysis, as shown in Fig. 7(c) and (d). As it could be expected, both samples were composed of dense agglomerate particles with large size. A slight difference is that the surface of Li-SBA15-10 sample was a bit rougher. This morphology was related to the high calcination temperature and was in agreement with previous literature reports.<sup>17, 20, 23, 31</sup>

### **3.4 CO<sub>2</sub> sorption performances of optimized sorbents**

#### **3.4.1 The influence of CO<sub>2</sub> concentration**

Considering the practical applications of CO<sub>2</sub> sorbents, the influence of CO<sub>2</sub> concentration on the sorption performance of optimized Li-SBA15-4 and Li-SBA15-10 samples was then investigated. Fig. 8(a) and (b) show the influence of CO<sub>2</sub> concentration on sorption performances of Li-SBA15-4 and Li-SBA15-10 samples at the same sorption temperature of 650 °C, respectively. For Li-SBA15-4 sample, it was evident that the sorption capacity dramatically dropped with the decrease in CO<sub>2</sub> concentration, particularly when the CO<sub>2</sub> concentration was 20 vol%. When the CO<sub>2</sub> concentration was 100 vol%, the CO<sub>2</sub> sorption capacity was as high as 36.7 wt%. However, it was decreased to only 25.8 wt% and 0.7 wt% when the CO<sub>2</sub> concentration was 50 vol% and 20 vol%, respectively. A similar CO<sub>2</sub> sorption performance was observed with Li-SBA15-10 sample as well. The CO<sub>2</sub> sorption capacity dropped sharply from 62.0 wt% to 37.8 wt% as the CO<sub>2</sub> concentration decreased from 100 vol%



to 50 vol%. However, the capacity did not decrease much with a further decrease in CO<sub>2</sub> concentration from 50 vol% to 20 vol%. This variation may be attributed to a reversible CO<sub>2</sub> sorption/desorption reaction occurring during the process, where the reverse reaction (CO<sub>2</sub> desorption) will be accelerated at high temperatures.<sup>25</sup>

Moreover, the sorption temperature should be lower since CO<sub>2</sub> sorption is an exothermic reaction from the viewpoint of equilibrium.<sup>41</sup> To elucidate this hypothesis, Temperature programmed sorption of CO<sub>2</sub> analysis was performed to determine the optimal sorption temperature under different CO<sub>2</sub> concentrations. In this temperature programmed process, samples were heated from room temperature to 800 °C at a ramping rate of 10 °C/min under different CO<sub>2</sub> concentrations, as shown in Fig. 8(c) and (d). All samples displayed similar profiles that the weight of samples first increased due to sorption and then sharply decreased once the reverse reaction was activated at one equilibrium temperature as the temperature increased. For Li-SBA15-4 sample, it was evident that the maximum peak temperature shifted to lower values with the decrease in CO<sub>2</sub> concentration. When the CO<sub>2</sub> concentration was low, it can be expected that a sorption temperature of 650 °C is too high to adsorb CO<sub>2</sub> so that it showed worse sorption performance in Fig. 8(a). However, for Li-SBA15-10 samples, the shift of the peak temperature was not obvious (Fig. 8(d)).

Thus, to improve their sorption performances under certain CO<sub>2</sub> atmosphere, selecting a proper sorption temperature is important. In Fig. 8(e), under 20 vol% CO<sub>2</sub> atmosphere, Li-SBA15-4 sample exhibited extremely low capacity at 625 °C (2.0 wt%) and 650 °C (0.7 wt%). However, its CO<sub>2</sub> sorption capacity was dramatically increased

to 29.5 wt% once the sorption temperature was decreased to 575 °C, being superior when compared with similar literature reports.<sup>14, 25, 26, 32, 41</sup> Under 50 vol% CO<sub>2</sub> atmosphere, the optimal sorption temperature was 600 °C for Li-SBA15-4 sample, with the highest CO<sub>2</sub> sorption capacity of 29.9 wt% (Fig. 8(f)). These results clearly demonstrated that the sorption performance of Li-SBA15-4 sample was highly dependent on both the CO<sub>2</sub> concentration and the sorption temperature.

Fig. 8(g) and (h) show the sorption performance of Li-SBA15-10 sample under 20 vol% and 50 vol% CO<sub>2</sub> atmosphere, respectively. It is obvious that both cases displayed slow kinetics when the sorption temperature was low (600 °C). While elevated temperature (750 °C) led to a reduced equilibrate capacity. The optimal sorption temperature was 650 °C for both cases, with the highest capacity of 36.4 wt% and 37.8 wt% for 20 vol% and 50 vol% CO<sub>2</sub> concentrations, respectively. The influence of CO<sub>2</sub> concentration for Li-SBA15-10 sample is different from that for Li-SBA15-4, which is still a mystery for us. We suspect that the sorption of CO<sub>2</sub> on the Li-SBA15-10 sample is more complex and might involve multiple steps. In generally, it can be concluded that the CO<sub>2</sub> sorption performance became worse to certain extent with the decrease in CO<sub>2</sub> concentration. In order to have good CO<sub>2</sub> sorption performance under low CO<sub>2</sub> concentrations, a relatively lower and proper sorption temperature should be selected.

### **3.4.2 The cycling stability test of the optimized samples**

The cycling stability is a decisive factor for the practical use of CO<sub>2</sub> sorbents. To evaluate the regeneration property and thermal stability of the optimized Li-SBA15-4 and Li-SBA15-10 samples, CO<sub>2</sub> sorption/desorption cycling tests were performed.

Before performing the cycling tests, the suitable desorption temperatures for both Li-SBA15-4 and Li-SBA15-10 samples were determined by temperature programmed desorption using TGA, as shown in Fig. 9(a) and (b). For Li-SBA15-4 sample, the sorbed CO<sub>2</sub> mainly desorbed in the temperature range of 600 to 650 °C, indicating that the suitable desorption temperature should be chosen at 600–650 °C. At these temperatures, the sorbed CO<sub>2</sub> can be completely desorbed from sample in a very short duration. Taking the sorption temperature of 650 °C into account, we selected 650 °C as the desorption temperature for Li-SBA15-4 sample. However, for Li-SBA15-10 sample, even with a temperature as high as 900 °C, the weight of sample only decreased 17.6 wt%, which was much less than its sorption capacity. For a comparison, we chose 650 °C as the desorption temperature for Li-SBA15-10 sample as well.

For Li-SBA15-4 sample, the sorption capacity reached 32.5 wt% for the third cycle, and maintained at 31.5 wt% even after 15 cycles. After 15 cycles, only 1 wt% capacity was lost, suggesting that the Li-SBA15-4 sample has excellent regeneration property and thermal stability. However, for Li-SBA15-10 sample, only 10.5 wt% of reversible CO<sub>2</sub> sorption/desorption capacity was obtained from its second cycle. Bad performance in multi-cycles weakened its potential application, and more investigations are needed to improve its performance in future.

In Fig. 9(c), Li-SBA15-4 showed excellent cycling performance with 100 vol% CO<sub>2</sub>. In this section, we further studied its CO<sub>2</sub> sorption/desorption cycling performance with lower CO<sub>2</sub> concentrations, which is more meaningful for practical applications, as shown in Fig. 9(e). With 50 vol% CO<sub>2</sub> atmosphere, both the CO<sub>2</sub>

sorption and desorption were conducted at 600 °C, with a capacity of 27.4 wt% after 15 cycles. As the CO<sub>2</sub> concentration was decreased to 20 vol%, the capacity also dropped to 18.2 wt% after 15 cycles at 575 °C. It is also apparent that more cycles are needed for the Li-SBA15-4 sorbent to achieve its equilibrium capacity with the decrease in CO<sub>2</sub> concentration. It can also be concluded that the CO<sub>2</sub> concentration has a great influence on the sorption and desorption performance of sorbents.

### **3.5 CO<sub>2</sub> sorption kinetics and mechanism**

#### **3.5.1 CO<sub>2</sub> sorption kinetics**

For kinetic study, we fitted the CO<sub>2</sub> sorption curves of Li-SBA15-4 and Li-SBA15-10 with suitable mathematical models for getting more information about their sorption properties. For Li-SBA15-4 sample, Li<sub>4</sub>SiO<sub>4</sub> is the main composition phase. It is well accepted that a double exponential model can be applied to fit the sorption curves of Li<sub>4</sub>SiO<sub>4</sub><sup>3, 31, 42</sup>, which assumes that two different sorption processes occur in the whole sorption. The diffusion process is the limit phenomenon once the external layer of mixed solid forms after initial carbonate reaction. The expression of the double exponential model can be expressed in equation (4),<sup>42</sup> where  $y$  represents the CO<sub>2</sub> sorption capacity in the form of mass percentage,  $t$  is the sorption time in second,  $k_1$  and  $k_2$  are the kinetic parameters in the surface chemical reaction and bulk diffusion process, respectively. Constants  $A$  and  $B$  are the intervals at the each process that controls the whole CO<sub>2</sub> sorption process.  $C$  indicates the y-intercept. All the kinetic analysis data are summarized in Table 3. Sample synthesized from SBA-15 and SiO<sub>2</sub> both had a high  $k_1$  value that was one order of magnitude higher than  $k_2$  value, which

indicates that the bulk diffusion process was the limit step during the whole process.<sup>3,</sup>  
<sup>15, 16, 21, 32</sup> Table 3 shows that both samples synthesized from SBA-15 and SiO<sub>2</sub> had similar performance during the initial carbonate reaction. However, the sample synthesized from SBA-15 displayed an excellent kinetics that was more than twice as fast as that of the sample synthesized from SiO<sub>2</sub>.

$$y = Aexp^{-k_1t} + Bexp^{-k_2t} + C \quad (4)$$

For the Li-SBA15-10 sample, the main phase was Li<sub>8</sub>SiO<sub>6</sub> which may involve a much complicated reaction mechanism than Li<sub>4</sub>SiO<sub>4</sub> and is therefore not suitable for the exponential model. Considering that the reaction conducted under the excess CO<sub>2</sub> atmosphere, a first-order reaction can be expected at the beginning of the reaction in a short time.<sup>34</sup> The first-order reaction is expressed in equation (5). Where  $m$  and  $m_0$  represent the sample mass during and before sorption process, respectively,  $t$  is the sorption time in second, and  $k$  is the kinetics constant. Fig. 10(a) shows that the plots of  $\ln\left(\frac{m}{m_0}\right)$  as a function of time for Li-SBA15-10 and Li-SiO<sub>2</sub>-10 samples. It was obvious that the Li-SBA15-10 sample possesses a much higher slope than that for Li-SiO<sub>2</sub>-10, demonstrating that Li-SBA15-10 possesses a much faster sorption rate.

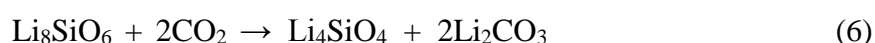
$$\ln\left(\frac{m}{m_0}\right) = kt \quad (5)$$

### 3.5.2 Reaction mechanism

To know about the reaction mechanism of those optimized samples, the products after sorption were analyzed further. Li-SBA15-4 sample was obtained by calcining at 750 °C for 2 h and Li-SBA15-10 sample was obtained by calcining at the same temperature for 4 h. Fig.10 (b) shows the XRD patterns of these samples after CO<sub>2</sub> sorption at 650

°C for 3 h, which indicate both samples produced  $\text{Li}_4\text{SiO}_4$ ,  $\text{Li}_2\text{SiO}_3$  and  $\text{Li}_2\text{CO}_3$  after sorption. For  $\text{Li}_4\text{SiO}_4$ , its theoretical  $\text{CO}_2$  sorption capacity according to reaction (5) is 36.7 wt%. The  $\text{CO}_2$  sorption capacity of our synthesized Li-SBA15-4 sample is 36.3 wt%, which accounts for 99% of its theoretical value.

For Li-SBA15-10 sample,  $\text{Li}_8\text{SiO}_6$  accounts for the major phase, as shown in Table 2. Fig. 10(b) confirms that no characteristic peak of  $\text{Li}_8\text{SiO}_6$  was detected after  $\text{CO}_2$  sorption, indicating a complete reaction of  $\text{Li}_8\text{SiO}_6$ . The possible reactions during the carbonation process was proposed in equation (6).<sup>30</sup> Considering the final products contain  $\text{Li}_4\text{SiO}_4$ ,  $\text{Li}_2\text{SiO}_3$  and  $\text{Li}_2\text{CO}_3$ , we propose that the  $\text{CO}_2$  sorption on  $\text{Li}_8\text{SiO}_6$  may occur according to the following route. 1 mole  $\text{Li}_8\text{SiO}_6$  sorbed 2 mole  $\text{CO}_2$  and produced 1 mole  $\text{Li}_4\text{SiO}_4$ , which can sequentially react further with  $\text{CO}_2$  to form  $\text{Li}_2\text{SiO}_3$  according to reaction (1). This means that  $\text{Li}_8\text{SiO}_6$  plays a significant role in the sharply rapid adsorption at the initial process of  $\text{CO}_2$  sorption on Li-SBA15-10 sorbents (Fig.4 (b)).



To prove this hypothesis, the products after only 5 min adsorption were analyzed by XRD and the whole adsorption curve of Li-SBA15-10 sorbents was fitted by stage by making use of kinetics models that apply to  $\text{Li}_8\text{SiO}_6$  and  $\text{Li}_4\text{SiO}_4$ , respectively. In Fig. 10(b), compared with raw Li-SBA15-10, no characteristic peak of  $\text{Li}_8\text{SiO}_6$  was detected after  $\text{CO}_2$  sorption for only 5 minutes, which indicated a complete and rapid reaction of  $\text{Li}_8\text{SiO}_6$  and meanwhile confirmed the hypothesis that  $\text{Li}_8\text{SiO}_6$  plays an significant role in the sharply rapid adsorption at the initial process of Li-SBA15-10

sorbents react with CO<sub>2</sub> (seen at Fig.4 (b)). From the viewpoint of kinetics, it is universal that a double exponential model is utilized to fit the whole sorption curve of Li<sub>4</sub>SiO<sub>4</sub> and a first-order reaction can be adapted to fit the sorption curve of Li<sub>8</sub>SiO<sub>6</sub> at the beginning of reaction in a short time.<sup>34, 42</sup> Hence, the whole adsorption curve of Li-SBA15-10 was fitted by stage with the two above models and relevant kinetics parameters can be seen in Table 3. The high *R* square indicated both models can fit the sorption curve well at different reaction processes, which further verified the hypothesis that Li<sub>8</sub>SiO<sub>6</sub> can adsorb CO<sub>2</sub> much faster than Li<sub>4</sub>SiO<sub>4</sub> in Li-SBA15-10. What's more, Li-SiO<sub>2</sub>-10 was also analyzed through the same method. However Li<sub>8</sub>SiO<sub>6</sub> or Li<sub>4</sub>SiO<sub>4</sub> reacted with CO<sub>2</sub>, Li-SBA15-10 was kept outstanding in a comparison with Li-SiO<sub>2</sub>-10, which demonstrated the advantage of SBA-15 in terms of kinetics.

It is well accepted that the double shell mechanism can be applied to describe the CO<sub>2</sub> sorption process on Li<sub>4</sub>SiO<sub>4</sub>.<sup>16, 38, 43, 44</sup> In the initial stage, a gas-solid reaction between Li<sub>4</sub>SiO<sub>4</sub> and CO<sub>2</sub> first occurred on the surface of Li<sub>4</sub>SiO<sub>4</sub> particles to produce Li<sub>2</sub>SiO<sub>3</sub> and Li<sub>2</sub>CO<sub>3</sub>, and with the reaction proceeding further, products accumulated to form a mixed solid layer surrounding unreacted Li<sub>4</sub>SiO<sub>4</sub>. Once the products layer was formed, the sorption of CO<sub>2</sub> on Li<sub>4</sub>SiO<sub>4</sub> will be dependent on the diffusion of lithium ions from the internal of Li<sub>4</sub>SiO<sub>4</sub> particle to the surface and the transport of CO<sub>2</sub> molecules through the products layer. However, Li<sub>8</sub>SiO<sub>6</sub> as a novel high-temperature CO<sub>2</sub> sorbent candidate has not yet been well investigated in detail. Combined with the above analysis, we proposed that the CO<sub>2</sub> entrapment in Li<sub>8</sub>SiO<sub>6</sub> might occur in two steps. First, Li<sub>8</sub>SiO<sub>6</sub> reacted with 2 mole CO<sub>2</sub> molecules to produce Li<sub>4</sub>SiO<sub>4</sub>, and second

$\text{Li}_4\text{SiO}_4$  further reacted with  $\text{CO}_2$  to form  $\text{Li}_2\text{SiO}_3$  and  $\text{Li}_2\text{CO}_3$ .

#### **4. Conclusions**

In this contribution, we demonstrated that SBA-15 can work as a superior silicon precursor than conventional  $\text{SiO}_2$  for the synthesis of alkali silicates with significantly improved  $\text{CO}_2$  capture performance. The Li/Si ratio, calcination temperature, and calcination duration showed great effect on the chemical composition and the  $\text{CO}_2$  capture capacity of obtained lithium silicates. XRD and a normalized reference intensity ratio analyses suggest that the  $\text{CO}_2$  sorption performance of synthesized lithium silicates can be correlated to their crystalline phase abundance. Under the optimized conditions, the Li-SBA15-4 sample that mainly contains  $\text{Li}_4\text{SiO}_4$  achieved an extremely high  $\text{CO}_2$  capture capacity of 36.3 wt%, by far the highest capacity among all reported  $\text{Li}_4\text{SiO}_4$  sorbents. Li-SBA15-4 also showed very high cycling stability with only 1.0 wt% capacity loss after 15 cycles. Another sample Li-SBA15-10 which mainly contains  $\text{Li}_8\text{SiO}_6$  displayed a very high  $\text{CO}_2$  uptake of 62.0 wt%, while its regeneration capacity was very poor, with only 10.5 wt% of reversible  $\text{CO}_2$  capture capacity. The influence of  $\text{CO}_2$  concentration (20%, 50%, and 100%) on the  $\text{CO}_2$  capture performance of Li-SBA15-4 and Li-SBA15-10 samples was also studied. At low  $\text{CO}_2$  concentrations, relatively lower sorption temperatures are needed for its maximum  $\text{CO}_2$  capture capacity. Kinetic studies showed that the lithium silicates synthesized from SBA-15 exhibited much higher kinetics parameter, which is more than twice as fast as that of the sample synthesized from  $\text{SiO}_2$ , suggesting SBA-15 as the silicon source promotes not only the  $\text{CO}_2$  sorption capacity but also sorption kinetics.



## Acknowledgements

This work was supported by the Fundamental Research Funds for the Central Universities (2016ZCQ03), the National Natural Science Foundation of China (51622801, 51572029, and 51308045), the Beijing Excellent Young Scholar (2015000026833ZK11), and the Xu Guangqi Grant.

## References

1. Wang, J.; Huang, L.; Yang, R.; Zhang, Z.; Wu, J.; Gao, Y.; Wang, Q.; O'Hare, D.; Zhong, Z., Recent advances in solid sorbents for CO<sub>2</sub> capture and new development trends. *Energy Environ. Sci.* **2014**, *7*, 3478.
2. Wang, Q.; Tay, H. H.; Guo, Z.; Chen, L.; Liu, Y.; Chang, J.; Zhong, Z.; Luo, J.; Borgna, A., Synthesis of high-temperature CO<sub>2</sub> adsorbents from organo-layered double hydroxides with markedly improved CO<sub>2</sub> capture capacity. *Energy Environ. Sci.* **2012**, *5*, 7526.
3. Kim, H.; Jang, H. D.; Choi, M., Facile synthesis of macroporous Li<sub>4</sub>SiO<sub>4</sub> with remarkably enhanced CO<sub>2</sub> adsorption kinetics. *Chem. Eng. J.* **2015**, *280*, 132.
4. Zheng, Q.; Huang, L.; Zhang, Y.; Wang, J.; Zhao, C.; Zhang, Q.; Zheng, W.; Cao, D.; O'Hare, D.; Wang, Q., Unexpected highly reversible topotactic CO<sub>2</sub> sorption/desorption capacity for potassium dititanate. *J. Mater. Chem.* **2016**, *4*, 12889.
5. Ridha, F. N.; Manovic, V.; Wu, Y.; Macchi, A.; Anthony, E. J., Post-combustion CO<sub>2</sub> capture by formic acid-modified CaO-based sorbents. *Int. J. Greenh. Gas Con.* **2013**, *16*, 21.
6. Veliz-Enriquez, M. Y.; Gonzalez, G.; Pfeiffer, H., Synthesis and CO<sub>2</sub> capture evaluation of Li<sub>2-x</sub>K<sub>x</sub>ZrO<sub>3</sub> solid solutions and crystal structure of a new lithium - potassium zirconate phase. *J. Solid State Chem.* **2007**, *180*, 2485.
7. Ochoa-Fernandez, E.; Ronning, M.; Grande, T.; Chen, D., Nanocrystalline Lithium Zirconate with Improved Kinetics for High-Temperature CO<sub>2</sub> Capture. *Chem. Mater.* **2006**, *18*, 1383.
8. Wang, J.; Huang, L.; Yang, R.; Zhang, Z.; Wu, J.; Gao, Y.; Wang, Q.; O'Hare, D.; Zhong, Z., Recent advances in solid sorbents for CO<sub>2</sub> capture and new development trends. *Energy Environ. Sci.* **2014**, *7*, (11), 3478.
9. K. Nakagawat, T. O., A novel method of CO<sub>2</sub> capture for high temperature gases. *J. Electrochem. Soc.* **1998**, *145*, (4), 1344.
10. Olivares-Marín, M. D., T. C. Maroto-Valer, M. Mercedes, Novel lithium-based sorbents from fly ashes for CO<sub>2</sub> capture at high temperatures. *Int. J. Greenh. Gas Con.* **2010**, *4*, (4), 623.
11. López Ortiz, A.; Escobedo Bretado, M. A.; Guzmán Velderrain, V.; Meléndez Zaragoza, M.; Salinas Gutiérrez, J.; Lardizábal Gutiérrez, D.; Collins-Martínez, V., Experimental and modeling kinetic study of the CO<sub>2</sub> absorption by Li<sub>4</sub>SiO<sub>4</sub>. *Int. J. Hydrogen Energy* **2014**, *39*, (29), 16656.

12. S. Shan, Q. J., L. Jiang, Q. Li, Y. Wang, J. Peng., Novel  $\text{Li}_4\text{SiO}_4$ -based sorbents from diatomite for high temperature  $\text{CO}_2$  capture. *Ceram. Int.* **2013**, (39), 5437.
13. Xiang, M.; Zhang, Y.; Hong, M.; Liu, S.; Zhang, Y.; Liu, H.; Gu, C.,  $\text{CO}_2$  absorption properties of Ti- and Na-doped porous  $\text{Li}_4\text{SiO}_4$  prepared by a sol–gel process. *J. Mater. Sci.* **2015**, 50, (13), 4698.
14. Lee, J. H.; Moon, B.; Kim, T. K.; Jeoung, S.; Moon, H. R., Thermal conversion of a tailored metal-organic framework into lithium silicate with an unusual morphology for efficient  $\text{CO}_2$  capture. *Dalton Trans.* **2015**, 44, (34), 15130.
15. Wang, K.; Yin, Z.; Zhao, P., Synthesis of macroporous  $\text{Li}_4\text{SiO}_4$  via a citric acid-based sol–gel route coupled with carbon coating and its  $\text{CO}_2$  chemisorption properties. *Ceram. Int.* **2016**, 42, (2), 2990.
16. Subha, P. V.; Nair, B. N.; Hareesh, P.; Mohamed, A. P.; Yamaguchi, T.; Warriar, K. G. K.; Hareesh, U. S., Enhanced  $\text{CO}_2$  absorption kinetics in lithium silicate platelets synthesized by a sol–gel approach. *J. Mater. Chem. A* **2014**, 2, (32), 12792.
17. Durán-Muñoz, F.; Romero-Ibarra, I. C.; Pfeiffer, H., Analysis of the  $\text{CO}_2$  chemisorption reaction mechanism in lithium oxosilicate ( $\text{Li}_8\text{SiO}_6$ ): a new option for high-temperature  $\text{CO}_2$  capture. *J. Mater. Chem. A* **2013**, 1, (12), 3919.
18. Haidong Zhang; Li, X., Novel mesoporous silica materials with hierarchically ordered nanochannel: a synthesis with the assistance of straight-chain alkanes and application. *J. Chem.* **2016**, 2016, 16.
19. Beltrán-Osuna, Á. A.; Perilla, J. E., Colloidal and spherical mesoporous silica particles: synthesis and new technologies for delivery applications. *J. Sol-Gel Sci. Technol.* **2015**, 77, (2), 480.
20. Wang, K. G., X. Zhao, P. Wang, F. Zheng, C., High temperature capture of  $\text{CO}_2$  on lithium-based sorbents from rice husk ash. *J. Hazard. Mater.* **2011**, 189, (1-2), 301.
21. Shan, S.; Jia, Q.; Jiang, L.; Li, Q.; Wang, Y.; Peng, J., Preparation and kinetic analysis of  $\text{Li}_4\text{SiO}_4$  sorbents with different silicon sources for high temperature  $\text{CO}_2$  capture. *Chin. Sci. Bull.* **2012**, 57, (19), 2475.
22. Wang, K.; Zhao, P.; Guo, X.; Han, D.; Chao, Y., High temperature capture of  $\text{CO}_2$  on  $\text{Li}_4\text{SiO}_4$ -based sorbents from biomass ashes. *Environ. Prog. Sustain. Energy* **2015**, 34, (2), 526.
23. Wang, K.; Zhao, P.; Guo, X.; Li, Y.; Han, D.; Chao, Y., Enhancement of reactivity in  $\text{Li}_4\text{SiO}_4$ -based sorbents from the nano-sized rice husk ash for high-temperature  $\text{CO}_2$  capture. *Energy Convers. Manage.* **2014**, 81, 447.
24. M.Kato, S. Y., K.Nakagawa, Carbon dioxide absorption by lithium orthosilicate in a wide range of temperature and carbon dioxide concentrations. *J. Mater.Sci. Lett.* **2002**, 21, 458.
25. Seggiani, M.; Puccini, M.; Vitolo, S., High-temperature and low concentration  $\text{CO}_2$  sorption on  $\text{Li}_4\text{SiO}_4$  based sorbents: Study of the used silica and doping method effects. *Int. J. Greenh. Gas Con.* **2011**, 5, (4), 741.
26. Seggiani, M.; Puccini, M.; Vitolo, S., Alkali promoted lithium orthosilicate for  $\text{CO}_2$  capture at high temperature and low concentration. *Int. J. Greenh. Gas Con.* **2013**, 17, 25.
27. Zhang, S.; Zhang, Q.; Wang, H.; Ni, Y.; Zhu, Z., Absorption behaviors study on doped  $\text{Li}_4\text{SiO}_4$  under a humidified atmosphere with low  $\text{CO}_2$  concentration. *Int. J. Hydrogen Energy* **2014**, 39, (31), 17913.
28. Gauer, C, H. W., Doped lithium orthosilicate for absorption of carbon dioxide. *J. Mater. Sci.* **2006**, 41, (8), 2405.
29. Ortiz-Landeros, J.; Gomez-Yanez, C.; Palacios-Romero, L. M.; Lima, E.; Pfeiffer, H., Structural and thermochemical chemisorption of  $\text{CO}_2$  on  $\text{Li}_{(4+x)}(\text{Si}_{(1-x)}\text{Al}_{(x)})\text{O}_4$  and

- $\text{Li}_{(4-x)}(\text{Si}_{(1-x)}\text{V}_{(x)})\text{O}_4$  solid solutions. *J. Phys. Chem. A* **2012**, *116*, (12), 3163.
30. Victoria L. Mejía-Trejo, E. F.-I., Heriberto Pfeiffer, Textural, structural, and  $\text{CO}_2$  chemisorption effects produced on the lithium orthosilicate by its doping with sodium ( $\text{Li}_{4-x}\text{Na}_x\text{SiO}_4$ ). *Chem. Mater.* **2008**, *20*, 7171.
  31. Romero-Ibarra, I. C.; Ortiz-Landeros, J.; Pfeiffer, H., Microstructural and  $\text{CO}_2$  chemisorption analyses of  $\text{Li}_4\text{SiO}_4$ : effect of surface modification by the ball milling process. *Thermochim. Acta* **2013**, *567*, 118.
  32. Sanna, A.; Ramli, I.; Mercedes Maroto-Valer, M., Development of sodium/lithium/fly ash sorbents for high temperature post-combustion  $\text{CO}_2$  capture. *Appl. Energ.* **2015**, *156*, 197.
  33. Yin, Z.; Wang, K.; Zhao, P.; Tang, X., Enhanced  $\text{CO}_2$  chemisorption properties of  $\text{Li}_4\text{SO}_4$ , using a water hydration–calcination technique. *Ind. Eng. Chem. Res.* **2016**, *55*, (4), 1142.
  34. Romero-Ibarra, I. C.; Durán-Muñoz, F.; Pfeiffer, H., Influence of the K-, Na- and K-Na-carbonate additions during the  $\text{CO}_2$  chemisorption on lithium oxosilicate ( $\text{Li}_8\text{SiO}_6$ ). *Greenhouse Gases Sci Technol.* **2014**, *4*, (1), 145.
  35. Jan Roggenbuck, G. K., Michael Tiemann, Synthesis of mesoporous magnesium oxide by CMK-3 carbon structure replication. *Chem. Mater.* **2006**, *18*, 4151.
  36. Zhao, D., Triblock copolymer syntheses of mesoporous silica with periodic 50 to 300 angstrom pores. *Science* **1998**, *279*, (5350), 548.
  37. Ding, Y.; Yin, G.; Liao, X.; Huang, Z.; Chen, X.; Yao, Y.; Li, J., A convenient route to synthesize SBA-15 rods with tunable pore length for lysozyme adsorption. *Microporous Mesoporous Mater.* **2013**, *170*, 45.
  38. Ortiz-Landeros, J.; Ávalos-Rendón, T. L.; Gómez-Yáñez, C.; Pfeiffer, H., Analysis and perspectives concerning  $\text{CO}_2$  chemisorption on lithium ceramics using thermal analysis. *J. Therm. Anal. Calorim.* **2011**, *108*, (2), 647.
  39. C., F. H., Quantitative interpretation of X-ray diffraction patterns of mixtures. II. adiabatic principle of X-ray diffraction analysis of mixtures. *J. Appl. Cryst.* **1974**, *7*, 526.
  40. Omotoso Oladipo, M. D. K., Hillier Stephen, Kleeberg Reinhard., Some successful approaches to quantitative mineral analysis as revealed by the 3<sup>rd</sup> Reynolds Cup contest. *Clays Clay Miner.* **2006**, *54*, (6), 748.
  41. K. Essaki, M. K., Influence of temperature and  $\text{CO}_2$  concentration on the  $\text{CO}_2$  absorption properties of lithium silicate pellets. *J. Mater. Sci.* **2005**, *40*, (18), 5017.
  42. Qi, Z.; Daying, H.; Yang, L.; Qian, Y.; Zibin, Z., Analysis of  $\text{CO}_2$  sorption/desorption kinetic behaviors and reaction mechanisms on  $\text{Li}_4\text{SiO}_4$ . *AIChE J.* **2013**, *59*, (3), 901.
  43. Xu, H.; Cheng, W.; Jin, X.; Wang, G.; Lu, H.; Wang, H.; Chen, D.; Fan, B.; Hou, T.; Zhang, R., Effect of the particle size of quartz powder on the synthesis and  $\text{CO}_2$  absorption properties of  $\text{Li}_4\text{SiO}_4$  at high temperature. *Ind. Eng. Chem. Res.* **2013**, *52*, (5), 1886.
  44. Amorim, S. M.; Domenico, M. D.; Dantas, T. L. P.; José, H. J.; Moreira, R. F. P. M., Lithium orthosilicate for  $\text{CO}_2$  capture with high regeneration capacity: kinetic study and modeling of carbonation and decarbonation reactions. *Chem. Eng. J.* **2016**, *283*, 388.

**Table 1.** Summary of silicate-based sorbents and their CO<sub>2</sub> capture performance.

Schemes	Materials	Synthesis conditions	CO <sub>2</sub> sorption performance	Ref.
Altering the silicon sources	Li <sub>4</sub> SiO <sub>4</sub>	solid-state route, rice husk ash, calcined at 800 °C for 4 h	32.4 wt% at 650 °C for 150 min, 100% CO <sub>2</sub> , 33.0 wt% after 15 cycles, sorption: 650 °C for 15 min, desorption: 800 °C for 10 min	20
		solid-state route, diatomite, calcined at 700 °C for 2 h	28.6 wt% at 620 °C for 180 min, 100% CO <sub>2</sub> , 32.3 wt% after 10 cycles, sorption and desorption at 700 °C for 30 min for each one	21
	Li <sub>4</sub> SiO <sub>4</sub>	solid-state route, diatomite, calcined at 700 °C for 2 h	30.3 wt% at 620 °C for 100 min, 50% CO <sub>2</sub> , 27.7 wt% after 16 cycles, sorption and desorption at 700 °C for 30 min for each one	12
	Li <sub>4</sub> SiO <sub>4</sub>	solid-state route, water pretreatment rice straw ash, calcined at 800 °C for 4 h	31.6 wt% at 680 °C for 120 min, 100% CO <sub>2</sub> , around 28.0 wt% after 15 cycles, sorption: 680 °C for 15 min, desorption: 800 °C for 10 min	22
		solid-state route, nano-citric acid pretreatment rice husk ash, calcined at 700 °C for 4 h	30.5 wt% at 680 °C for 120 min, 100% CO <sub>2</sub> , around 27.0 wt% after 15 cycles, sorption: 680 °C for 15 min, desorption: 800 °C for 10 min	23
designing special morphology	platelet-shaped Li <sub>4</sub> SiO <sub>4</sub>	sol-gel approach, colloidal silica, calcined at 800 °C for 3 h	35.0 wt% at 700 °C, 100% CO <sub>2</sub> , around 35.0 wt% after 5 cycles, sorption and desorption at 700 °C	16
	macroporous Li <sub>4</sub> SiO <sub>4</sub>	solid-state route, fumed silica (Cab-O-Sil, M5), calcined at 600 °C for 7 h	29.8 wt% at 550 °C for 100 min, 100% CO <sub>2</sub> , around 28.0 wt% after 10 cycles, sorption: 550 °C for 120 min, desorption: 550 °C for 300 min	3
	coral-like Li <sub>4</sub> SiO <sub>4</sub>	a metal-organic frameworks as	32.4 wt% at 550 °C for 300 min, 15% CO <sub>2</sub> ,	14

		precursors, calcined at 700 °C for 6 h and further calcined at 650 °C for 2 h	from 22.4 wt% to 7.7 wt% after 25 cycles, sorption: at 550 °C, desorption: at 650 °C, a cycle for 200 min	
	macroporous Li <sub>4</sub> SiO <sub>4</sub> coupled with carbon coating	a sol-gel method combined with carbon coating, fumed silica, calcined at 700 °C for 4 h	34.2 wt% at 680 °C for 120 min, 100% CO <sub>2</sub> , around 32.5 wt% after 20 cycles, sorption: 680 °C for 15 min, desorption: 800 °C for 10 min	15
	Li <sub>4</sub> SiO <sub>4</sub> +K <sub>2</sub> CO <sub>3</sub>	solid-state route, SiO <sub>2</sub> (quartz type), calcined at 1000 °C for 8 h	27.7 wt% at 500 °C for 60 min, 20% CO <sub>2</sub>	24
	Li <sub>4</sub> SiO <sub>4</sub> +K <sub>2</sub> CO <sub>3</sub>	solid-state route, fly ashes, calcined at 950 °C for 8 h	10.7 wt% at 600 °C for 60 min, 100% CO <sub>2</sub> , 10.1 wt% after 10 cycles, sorption and desorption at 600 °C for 15 min for each one	10
Loading with alkali metals	Li <sub>4</sub> SiO <sub>4</sub> +K <sub>2</sub> CO <sub>3</sub>	solid-state route, crystalline quartz, calcined at 900 °C for 4 h	27.0 wt% at 580 °C for 120 min, 4% CO <sub>2</sub> , 23.0 wt% after 4 cycles, sorption: 580 °C for 60 min, desorption: 750 °C for 10 min	25
	Li <sub>4</sub> SiO <sub>4</sub> +K <sub>2</sub> CO <sub>3</sub> +Na <sub>2</sub> CO <sub>3</sub>	solid-state route, quartz type, calcined at 900 °C for 4 h	23.0 wt% at 580 °C for 120 min, 4% CO <sub>2</sub> , for K-Li <sub>4</sub> SiO <sub>4</sub> , 15.0 wt% after 25 cycles, sorption: 580 °C for 30 min, desorption: 700 °C for 15 min	26
	Li <sub>4</sub> SiO <sub>4</sub> +K <sub>2</sub> CO <sub>3</sub>	solid-state route, SiO <sub>2</sub> (AR), calcined at 750 °C for 6 h	31.0 wt% at 575 °C for 200 min, 10% CO <sub>2</sub> , 20% steam, 22.5 wt% after 10 cycles, sorption: 575 °C, 100% CO <sub>2</sub> , desorption: 700 °C	27
Transition metal doping	Al and Fe doped Li <sub>4</sub> SiO <sub>4</sub>	solid-state route, SiO <sub>2</sub> (AR) , calcined at 850 °C for 8 h	22.0 wt% at 650 °C for 60 min, 100% CO <sub>2</sub> , 18.7 wt% after 5 cycles, sorption and desorption at 650 °C for 60 min for each one	28
	Li <sub>4+x</sub> (Si <sub>1-x</sub> Al <sub>x</sub> )O <sub>4</sub>	solid-state route, fumed silica, calcined at 850 °C	17.2 wt% at 700 °C for 200 min, 100% CO <sub>2</sub>	29

Li substitution by Na	$\text{Li}_{4-x}\text{Na}_x\text{SiO}_4$	for 12.5 h coprecipitation method, tetraethyl- orthosilicate, calcined at 900 °C for 6 h	19.4 wt% at 680 °C for 300 min, 100% CO <sub>2</sub>	30
	$\text{Li}_{3.9}\text{Na}_{0.1}\text{Si}_{0.96}\text{Ti}_{0.04}\text{O}_4$	a sol-gel method, tetraethyl orthosilicate, calcined at 700 °C for 4 h	31.6 wt% at 650 °C for 180 min, 100% CO <sub>2</sub> , 33.1 wt% after 10 cycles, sorption: 650 °C for 60 min, desorption: 650 °C for 40 min	13
	$\text{Li}_4\text{SiO}_4$ modified by the ball milling	wet-mixing and solid-state route, fumed silica, calcined at 700 °C for 4 h	21.1 wt% at 600 °C for 240 min, 100% CO <sub>2</sub> , 15.0 wt% after 10 cycles, sorption and desorption at 550 °C for 90 min for each one	31
	$\text{Li}_4\text{SiO}_4$	water-based sol- gel technique, SiO <sub>2</sub> (AR), calcined at 700 °C for 4 h	32.3 wt% at 680 °C for 120 min, 100% CO <sub>2</sub> , 28.6 wt% after 15 cycles, sorption: 680 °C for 15 min, desorption: 800 °C for 10 min	23
others	Fly ash based Na/Li silicates	solid-state route, fly ash, calcined at 800 °C for 8 h	16.2 wt% at 700 °C for 120 min, 14% CO <sub>2</sub> , 12% H <sub>2</sub> O, around 10 wt% after 10 cycles, sorption and desorption at 700 °C for 45 min for each other	32
	$\text{Li}_4\text{SiO}_4$	hydration–calcinat ion technique, fumed silica, calcined at 800 °C for 4 h	27.5 wt% at 680 °C for 120 min, 100% CO <sub>2</sub> , around 27.5 wt% after 15 cycles, sorption: 680 °C for 15 min, desorption: 800 °C for 10 min	33
$\text{Li}_8\text{SiO}_6$	$\text{Li}_8\text{SiO}_6$	solid-state reaction, silicon dioxide, calcined at 800 °C for 8 h	52.1 wt% at 650 °C for 180 min, 100% CO <sub>2</sub>	17
	$\text{Li}_8\text{SiO}_6 + \text{K}_2\text{CO}_3$ + $\text{Na}_2\text{CO}_3$	solid-state reaction, silicon dioxide, calcined at 800 °C for 8 h	45.0 wt% at 650 °C for 180 min, 100% CO <sub>2</sub> , 6.6 wt% after 10 cycles, sorption: 650 °C, desorption: 800 °C	34

**Table 2.** Phase abundance of all synthesized samples calculated by a normalized RIR method.

Calcination T (°C)	Calcination duration (h)	Samples	Chemical components (%)					
			Li <sub>8</sub> SiO <sub>6</sub>	Li <sub>4</sub> SiO <sub>4</sub>	Li <sub>2</sub> SiO <sub>3</sub>	LiOH	Li <sub>2</sub> O	SiO <sub>2</sub>
750	6	Li-SBA15-3	-	71.84	28.16	-	-	-
		Li-SBA15-4	-	98.09	1.91	-	-	-
		Li-SiO <sub>2</sub> -4	-	80.99	17.08	-	-	1.93
		Li-SBA15-5	-	100.00	-	-	-	-
		Li-SBA15-6	22.59	77.41	-	-	-	-
		Li-SBA15-7	40.33	59.67	-	-	-	-
		Li-SBA15-8	36.48	63.52	-	-	-	-
		Li-SBA15-9	30.23	34.90	-	34.87	-	-
		Li-SBA15-10	40.62	18.28	-	41.10	-	-
		Li-SBA15-11	57.32	36.62	-	-	6.06	-
	6	Li-SBA15-4	-	98.09	1.91	-	-	-
		Li-SBA15-10	40.62	18.28	-	41.10	-	-
	4	Li-SBA15-4	-	97.08	2.92	-	-	-
		Li-SBA15-10	58.78	19.88	-	21.34	-	-
		Li-SiO <sub>2</sub> -10	32.16	27.92	-	39.92	-	-
	2	Li-SBA15-4	-	92.13	7.87	-	-	-
		Li-SiO <sub>2</sub> -4	-	72.58	2.46	-	-	24.95
		Li-SBA15-10	17.47	36.36	-	46.16	-	-
	0.5	Li-SBA15-4	-	94.03	5.97	-	-	-
		Li-SBA15-10	11.25	31.98	-	45.22	11.54	-
650	2	Li-SBA15-4	-	93.92	6.08	-	-	-
750		Li-SBA15-4	-	92.13	7.87	-	-	-
850		Li-SBA15-4	-	93.87	6.13	-	-	-
650	4	Li-SBA15-10	24.45	75.55	-	-	-	-
750		Li-SBA15-10	58.78	19.88	-	21.34	-	-
850		Li-SBA15-10	15.66	57.63	-	-	26.70	-

**Table 3.** Kinetics parameters obtained from CO<sub>2</sub> sorption curve fittings for Li-SBA15-4, Li-SiO<sub>2</sub>-4, Li-SBA15-10, and Li-SiO<sub>2</sub>-10.

Samples	k <sub>1</sub>	k <sub>2</sub>	A	B	C	R <sup>2</sup>
Li-SBA15-4	0.0042	0.00078	-0.34	-0.078	0.36	0.9907
Li-SiO <sub>2</sub> -4	0.0040	0.00035	-0.15	-0.13	0.24	0.9954
Li-SBA15-10-S1*	0.0056	-	-	-	-	0.9965
Li-SiO <sub>2</sub> -10-S1*	0.0049	-	-	-	-	0.9981
Li-SBA15-10-S2*	0.0039	0.00026	-0.15	-0.04	0.18	0.9997
Li-SiO <sub>2</sub> -10-S2*	0.0018	0.00007	-0.17	-0.04	0.21	0.9999

\*S1 denotes the very beginning process within a short period of time and S2 denotes the rest process of the whole reaction for CO<sub>2</sub> sorption on Li<sub>8</sub>SiO<sub>6</sub>.



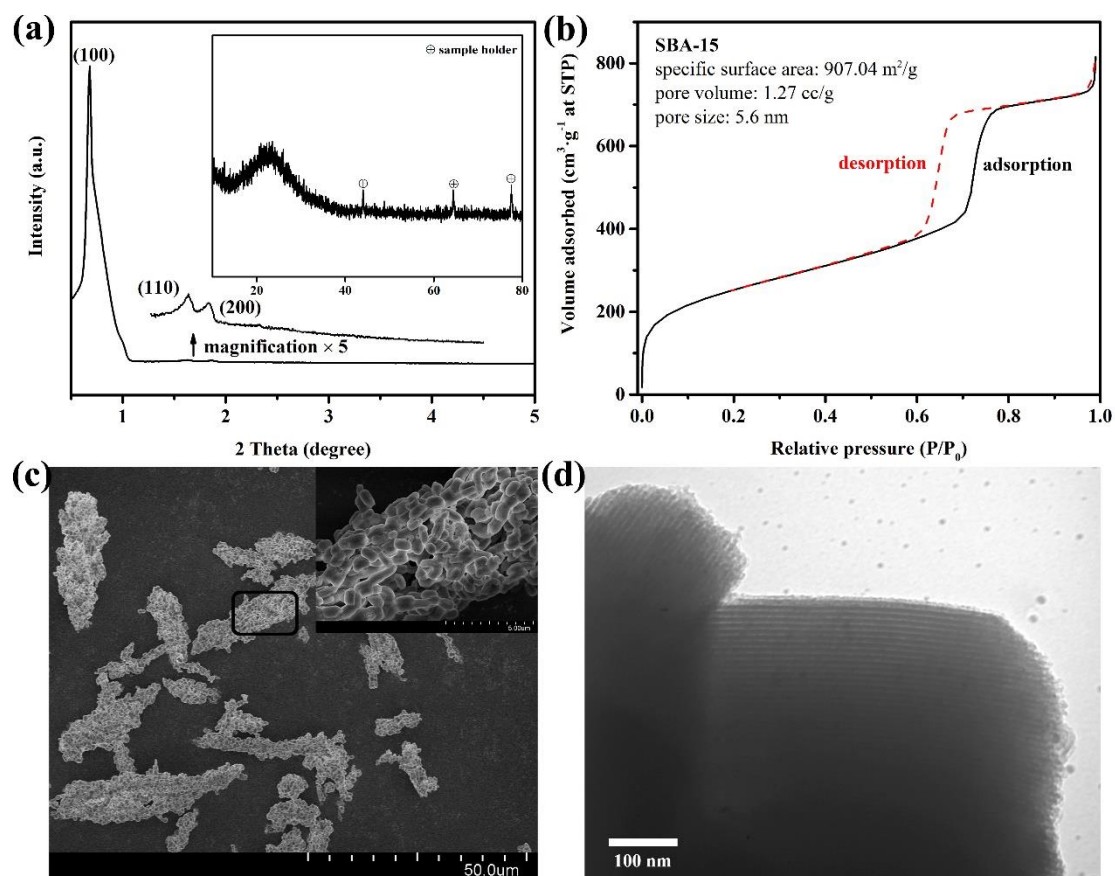


**Fig. 1.** (a) XRD patterns, (b)  $N_2$  adsorption/desorption isotherm, (c) SEM images, and (d) TEM image of synthesized SBA-15.

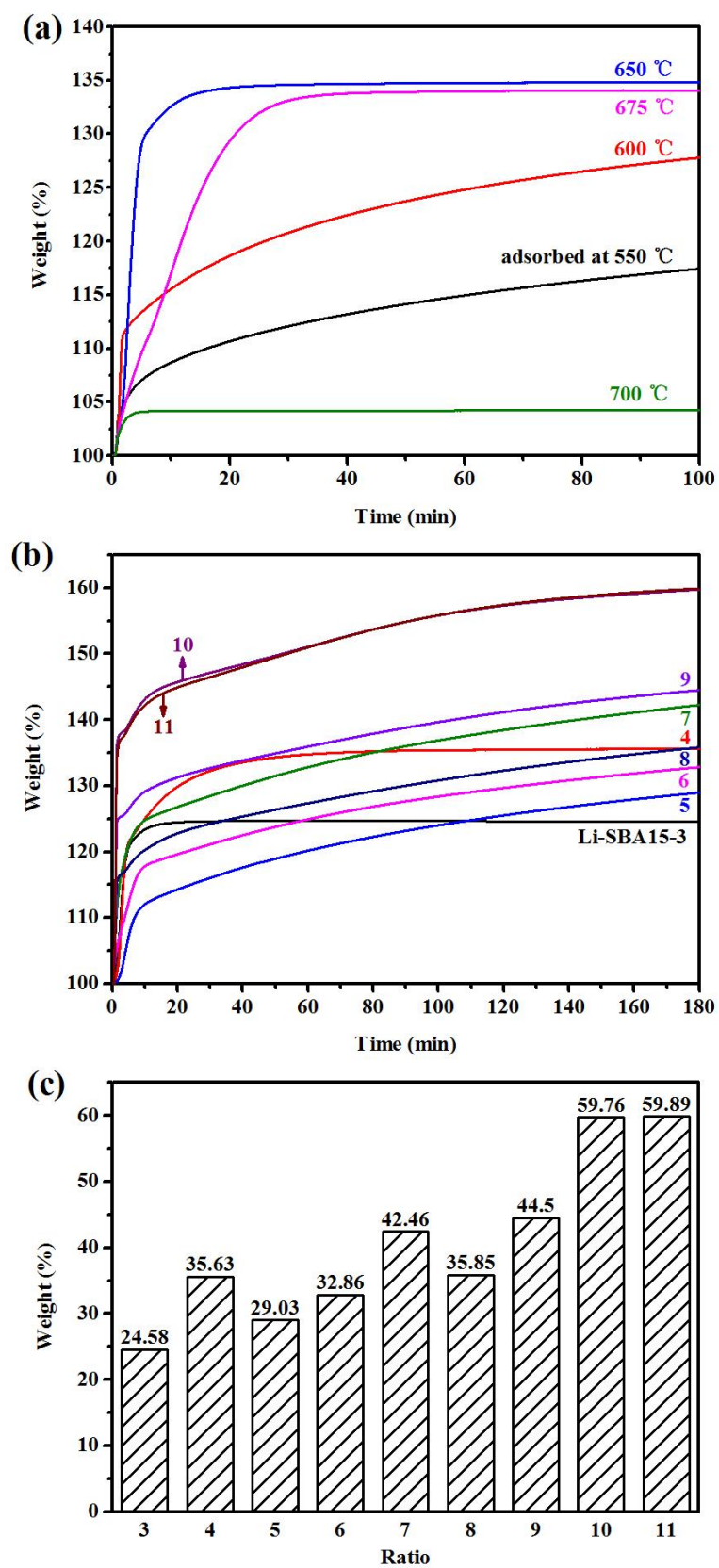


**Fig. 2.** (a) The effect of sorption temperature on the CO<sub>2</sub> capture performance of Li-SBA15-4 sample, and (b) and (c) the CO<sub>2</sub> capture capacity of Li-SBA15-*x* samples tested at 650 °C.

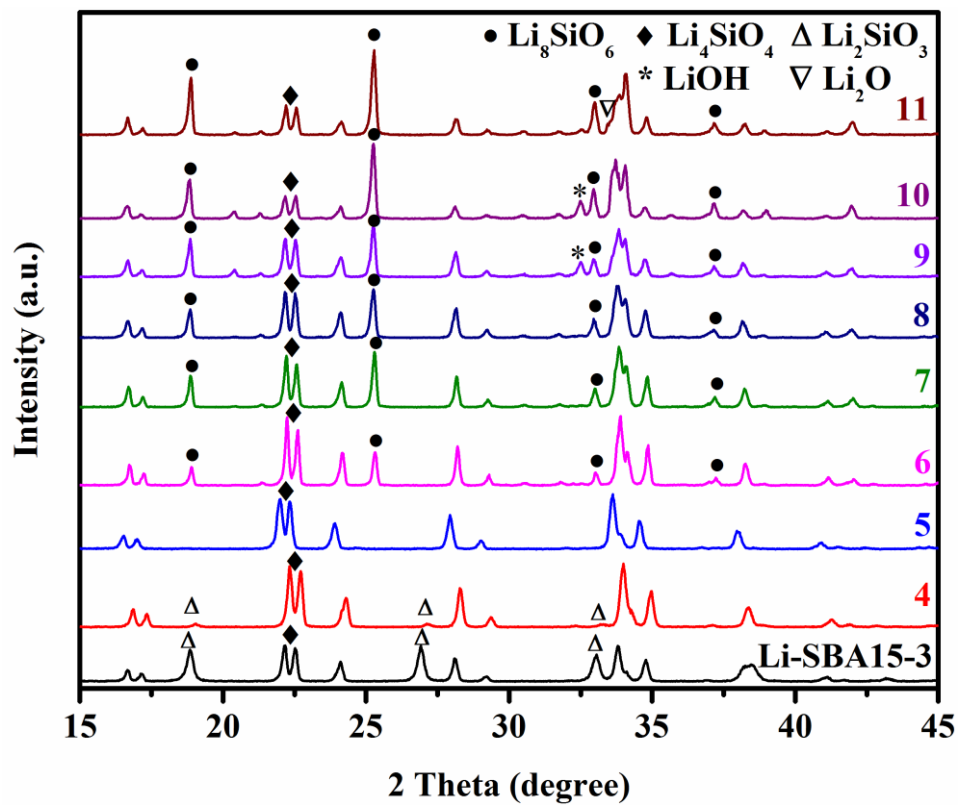


**Fig. 3.** XRD patterns of Li-SBA- $x$  samples with different Li/Si molar ratios from 3 to 11.

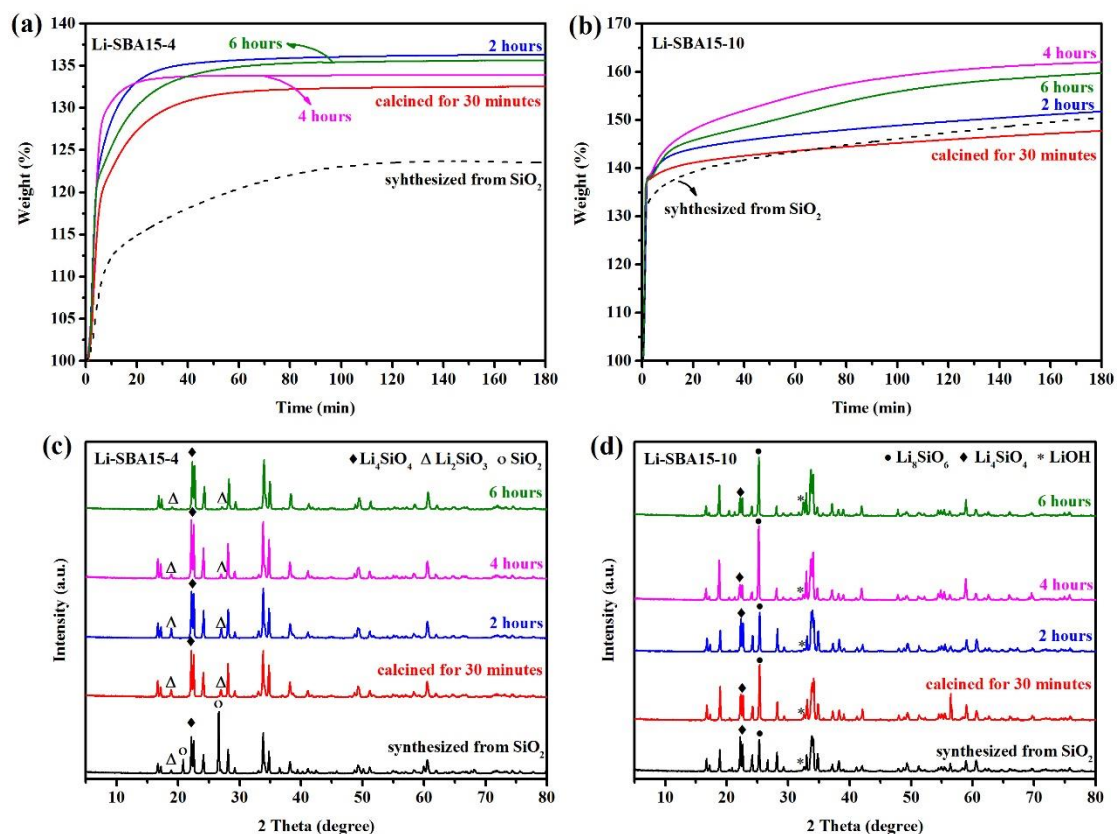


**Fig. 4.** CO<sub>2</sub> sorption isotherms of (a) Li-SBA15-4 samples and (b) Li-SBA15-10 samples calcined at 750 °C for different calcination durations, and XRD patterns of (c) Li-SBA15-4 samples and (d) Li-SBA15-10 samples calcined at 750 °C for different calcination durations.

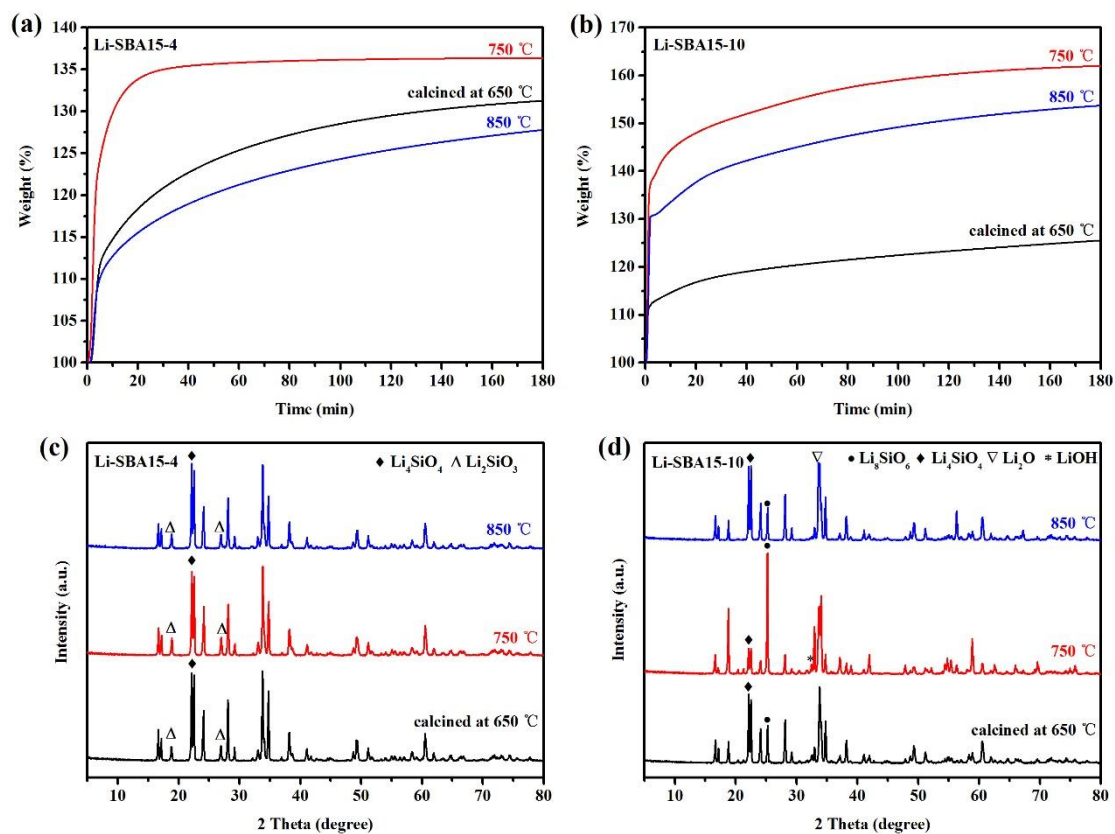


**Fig. 5.** The CO<sub>2</sub> sorption performance of (a) Li-SBA15-4 samples and (b) Li-SBA15-10 samples calcined at different calcination temperatures for 2 and 4 h, respectively, and XRD patterns of (c) Li-SBA15-4 samples and (d) Li-SBA15-10 samples calcined at different calcination temperatures for 2 and 4 h, respectively.

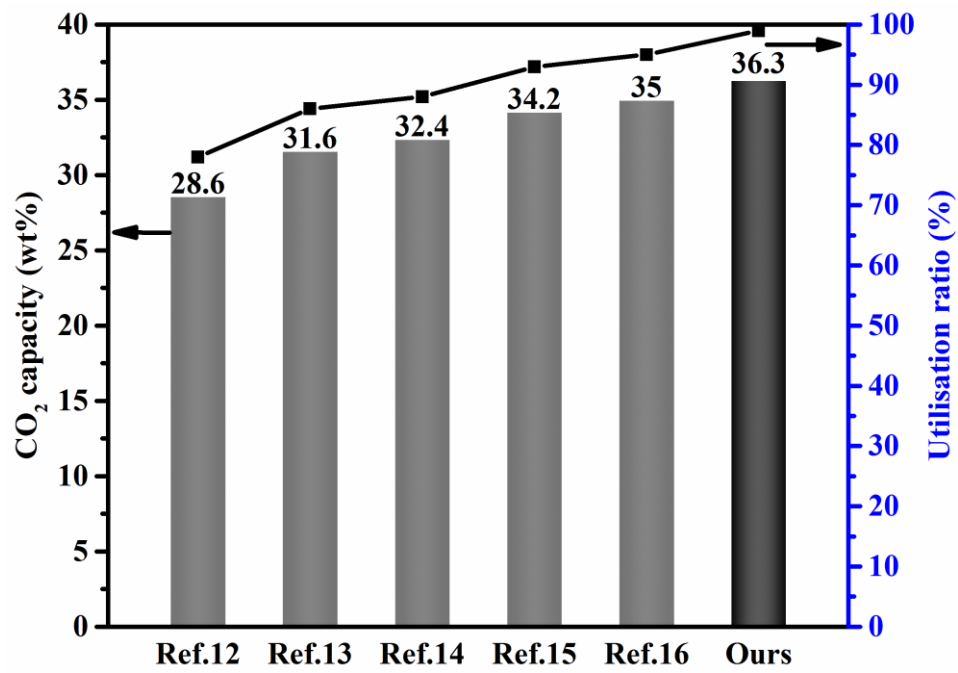


**Fig. 6.** Comparison of the CO<sub>2</sub> capture capacity of optimized Li-SBA15-4 (Li<sub>4</sub>SiO<sub>4</sub>) with other Li<sub>4</sub>SiO<sub>4</sub> samples that were reported in literatures.

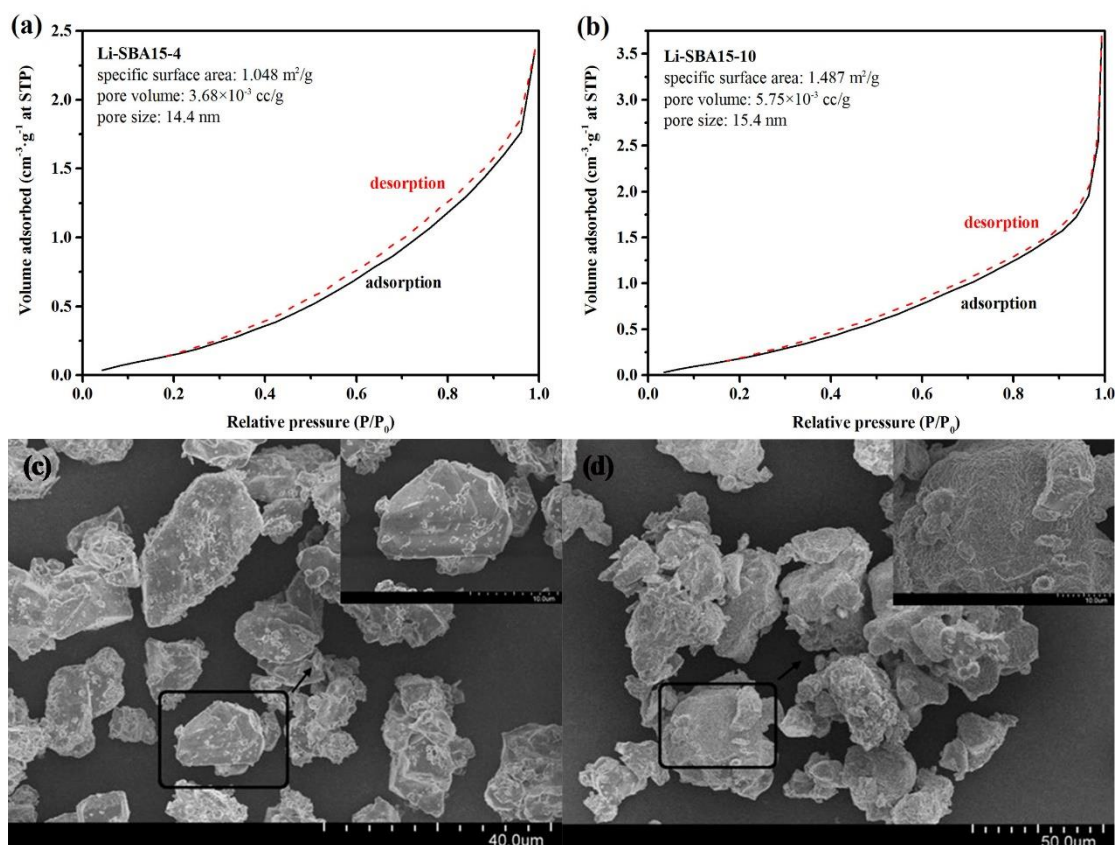


**Fig. 7.** N<sub>2</sub> adsorption/desorption isotherms of (a) Li-SBA15-4 synthesized at 750 °C for 2 h and (b) Li-SBA15-10 synthesized at 750 °C for 4 h, SEM images of (c) Li-SBA15-4 synthesized at 750 °C for 2 h and (d) Li-SBA15-10 synthesized at 750 °C for 4 h.



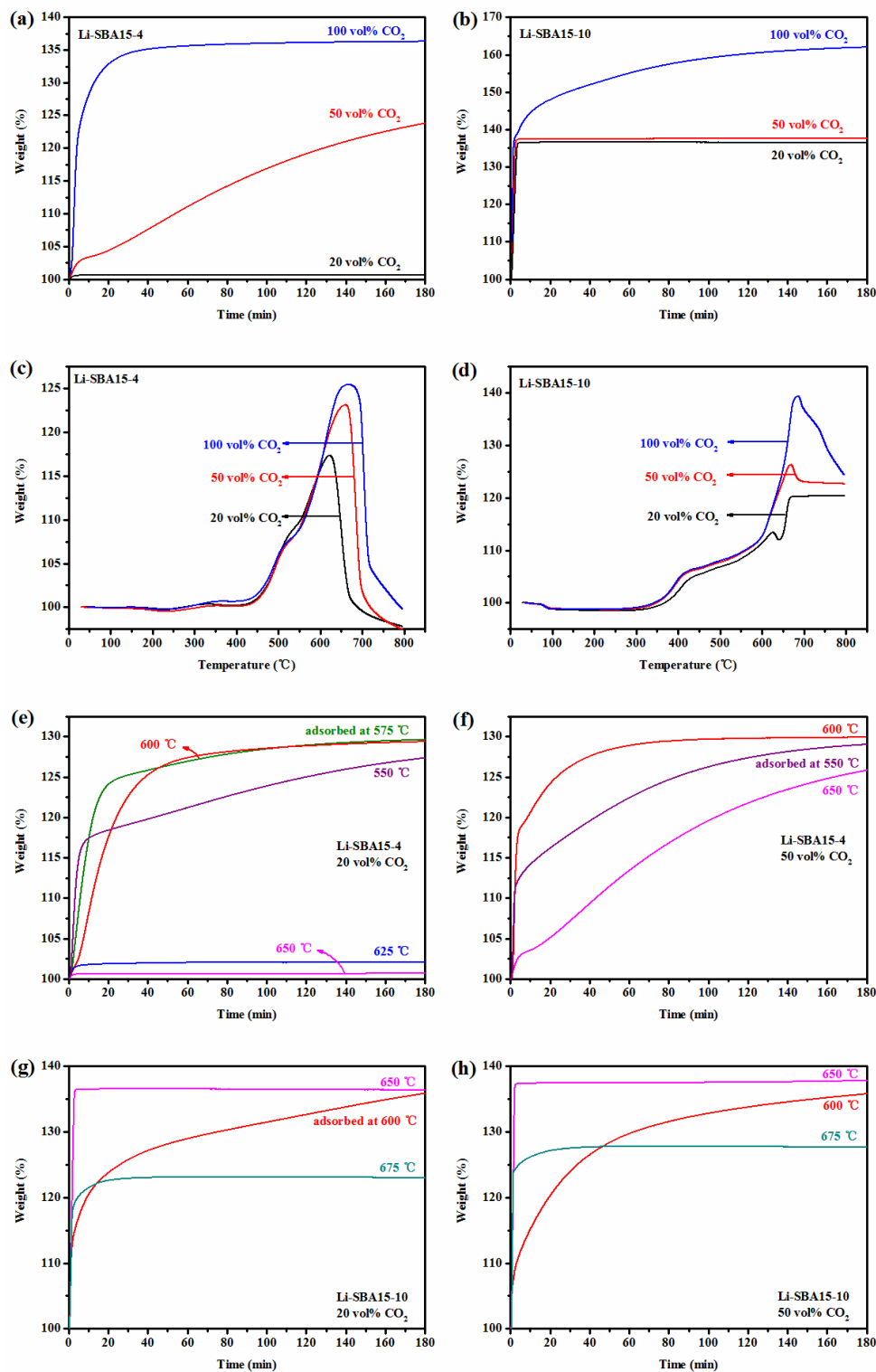


**Fig. 8.** CO<sub>2</sub> sorption isotherms of (a) optimized Li-SBA15-4 and (b) optimized Li-SBA15-10 samples under different CO<sub>2</sub> concentrations, respectively, temperature programmed adsorption of CO<sub>2</sub> for (c) optimized Li-SBA15-4 and (d) optimized Li-SBA15-10 samples under different CO<sub>2</sub> concentrations, respectively, CO<sub>2</sub> sorption isotherms at different sorption temperatures of optimized Li-SBA15-4 sample under the CO<sub>2</sub> concentration of (e) 20 vol% and (f) 50 vol%, respectively, and CO<sub>2</sub> sorption isotherms at different sorption temperatures of optimized Li-SBA15-10 sample under the CO<sub>2</sub> concentration of (g) 20 vol% and (h) 50 vol%, respectively.



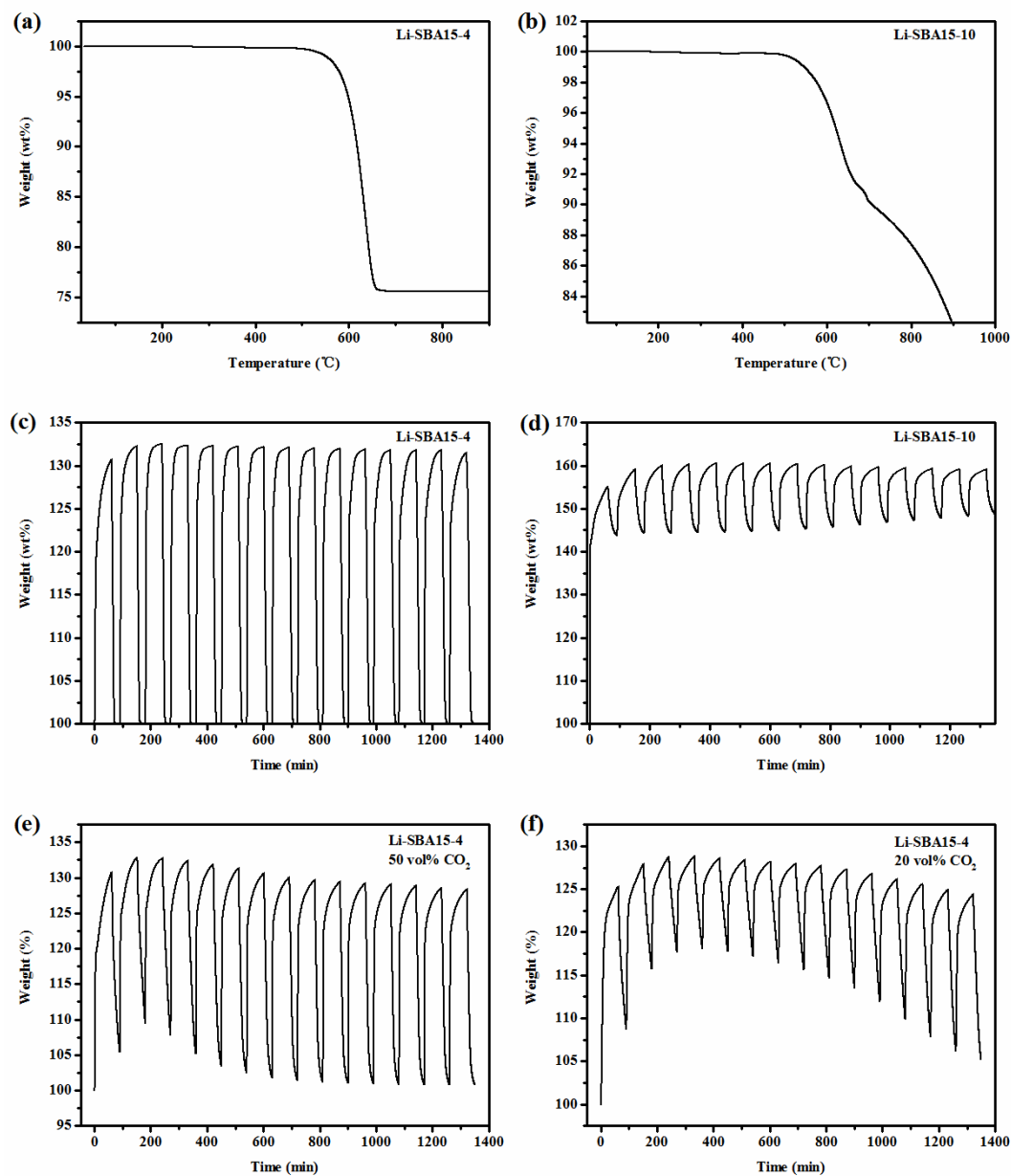


**Fig. 9.** Temperature program desorption of sorbed CO<sub>2</sub> on (a) Li-SBA15-4 and (b) Li-SBA15-10 samples, and CO<sub>2</sub> sorption/desorption cycling performance of (c) Li-SBA15-4 and (d) Li-SBA15-10 samples, and CO<sub>2</sub> sorption/desorption cycling performance of Li-SBA15-4 samples under (e) 50 vol% and (f) 20 vol% CO<sub>2</sub> atmosphere.

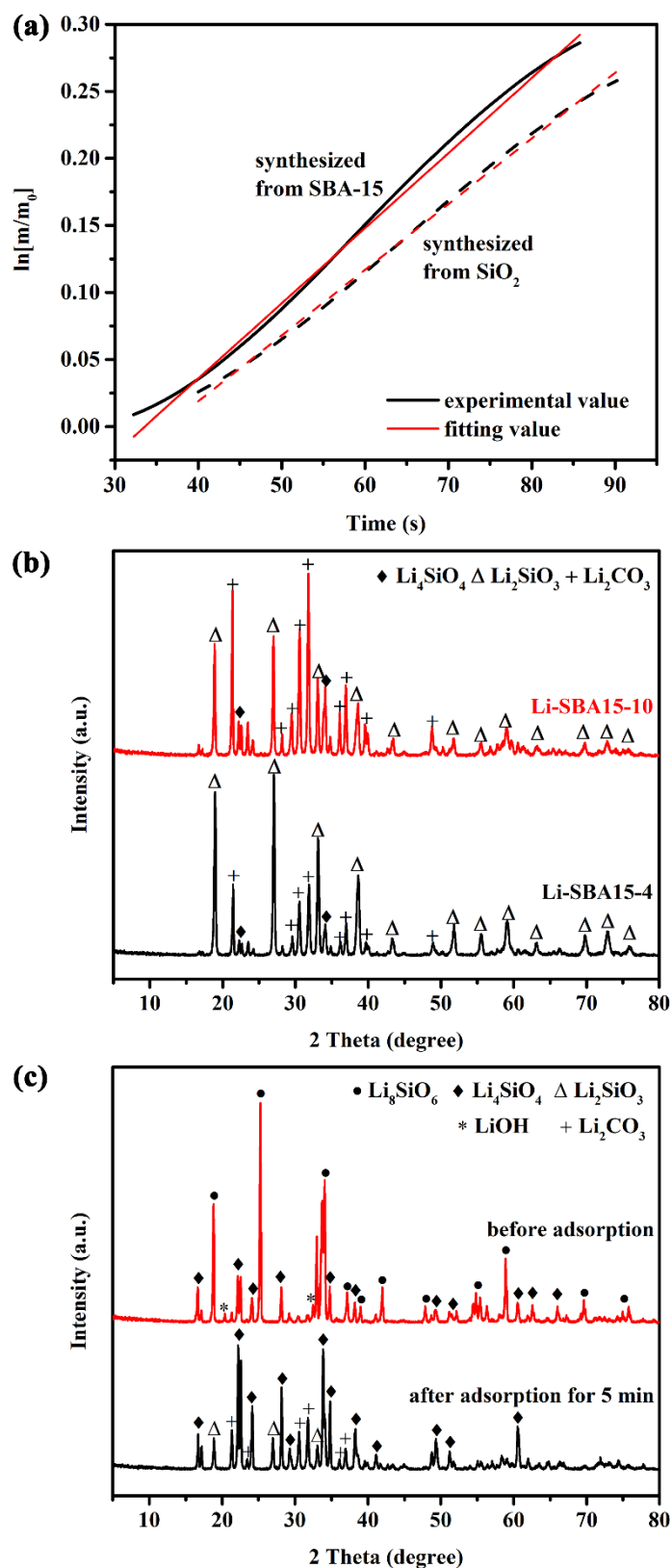


**Fig. 10.** (a) Plots of  $\ln[m/m_0]$  as a function of time for Li-SBA15-10 and Li-SiO<sub>2</sub>-10. Data obtained in an extremely short time, which may correspond to a stage where diffusion process did not occur. (b) XRD patterns of products after CO<sub>2</sub> sorption for 3 h from Li-SBA15-4 and Li-SBA15-10. (c) XRD patterns of products after CO<sub>2</sub> sorption on Li-SBA15-10 for only 5 minutes.